
Accelerated Linearized Laplace Approximation for Bayesian Deep Learning

Zhijie Deng^{1,2}, Feng Zhou^{2,3}, Jun Zhu² *

¹ Qing Yuan Research Institute, Shanghai Jiao Tong University

² Dept. of Comp. Sci. & Tech., BNRist Center, THU-Bosch Joint ML Center, Tsinghua University

³ Center for Applied Statistics, School of Statistics, Renmin University of China
zhijied@sjtu.edu.cn, feng.zhou@ruc.edu.cn, dcszj@tsinghua.edu.cn

Abstract

Laplace approximation (LA) and its linearized variant (LLA) enable effortless adaptation of pretrained deep neural networks to Bayesian neural networks. The generalized Gauss-Newton (GGN) approximation is typically introduced to improve their tractability. However, LA and LLA are still confronted with non-trivial inefficiency issues and should rely on Kronecker-factored, diagonal, or even last-layer approximate GGN matrices in practical use. These approximations are likely to harm the fidelity of learning outcomes. To tackle this issue, inspired by the connections between LLA and neural tangent kernels (NTKs), we develop a Nystrom approximation to NTKs to accelerate LLA. Our method benefits from the capability of popular deep learning libraries for forward mode automatic differentiation, and enjoys reassuring theoretical guarantees. Extensive studies reflect the merits of the proposed method in aspects of both scalability and performance. Our method can even scale up to architectures like vision transformers. We also offer valuable ablation studies to diagnose our method. Code is available at <https://github.com/thudzj/ELLA>.

1 Introduction

Deep neural networks (DNNs) excel at modeling deterministic relationships and have become *de facto* solutions for diverse pattern recognition problems [18, 54]. However, DNNs fall short in reasoning about model uncertainty [1] and suffer from poor calibration [17]. These issues are intolerable in risk-sensitive scenarios like self-driving [27], healthcare [34], finance [25], etc.

Bayesian Neural Networks (BNNs) have emerged as effective prescriptions to these pathologies [37, 21, 44, 16]. They usually proceed by estimating the posteriors over high-dimensional NN parameters. Due to some intractable integrals, diverse approximate inference methods have been applied to learning BNNs, spanning variational inference (VI) [1, 36], Markov chain Monte Carlo (MCMC) [55, 4], Laplace approximation (LA) [38, 50, 30], etc.

LA has recently gained unprecedented attention because its *post-hoc* nature nicely suits with the *pretraining-finetuning* fashion in deep learning (DL). LA approximates the posterior with a Gaussian around its maximum, whose mean and covariance are the *maximum a posteriori* (MAP) and the inversion of the Hessian respectively. It is a common practice to approximate the Hessian with the generalized Gauss-Newton (GGN) matrix [40] to make the whole workflow more tractable.

Linearized LA (LLA) [14, 22] applies LA to the first-order approximation of the NN of concern. Immer et al. [22] argue that LLA is more sensible than LA in the presence of GGN approximation;

*Corresponding author. Majority of work completed while Zhijie Deng was at Tsinghua University.

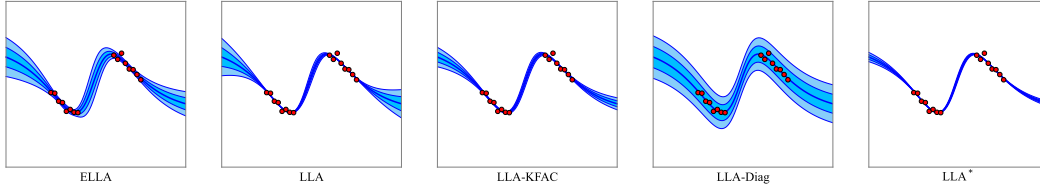


Figure 1: 1-D regression on $y = \sin 2x + \epsilon$, $\epsilon \sim \mathcal{N}(0, 0.2)$. Red dots, central blue curves, and shaded regions refer to the training data, mean predictions, and uncertainty respectively. The model is a pretrained multilayer perceptron (MLP) with 3 hidden layers. As shown, the predictive uncertainty of ELLA is on par with or better than the competitors such as LLA with KFAC approximation (LLA-KFAC), LLA with diagonal approximation (LLA-Diag), and last-layer LLA (LLA*).

LLA can perform on par with or better than popular alternatives on various uncertainty quantification (UQ) tasks [14, 6, 7]. The Laplace library [6] further substantially advances LLA’s applicability, making it a simple and competing baseline for Bayesian DL.

The practical adoption of LA and LLA actually entails further approximations on top of GGN. E.g., when using Laplace to process a pretrained ResNet [18], practitioners are recommended to resort to a Kronecker-factored (KFAC) [40] or diagonal approximation of the full GGN matrix for tractability. An orthogonal tactic is to apply LA/LLA to only NNs’ last layer [30]. Yet, the approximation errors in these cases can hardly be identified, significantly undermining the fidelity of the learning outcomes.

This paper aims at scaling LLA up to make probabilistic predictions in a more assurable way. We first revisit the inherent connections between Neural Tangent Kernels (NTKs) [24] and LLA [28, 22], and find that, if we can approximate the NTKs with the inner product of some low-dimensional vector representations of the data, LLA can be considerably accelerated. Given this finding, we propose to adapt the Nyström method to approximate the NTKs of multi-output NNs, and advocate leveraging forward mode automatic differentiation (*fwAD*) to efficiently compute the involved Jacobian-vector products (JVPs). The resultant *accelerated LLA (ELLA)* preserves the principal structures of vanilla LLA yet without explicitly computing/storing the costly GGN/Jacobian matrices for the training data. What’s more, we theoretically analyze the approximation error between the predictive of ELLA and that of vanilla LLA, and find that it decreases rapidly as the Nyström approximation becomes accurate.

We perform extensive studies to show that ELLA can be a low-cost and effective baseline for Bayesian DL. We first describe how to specify the hyperparameters of ELLA, and use an illustrative regression task to demonstrate the effectiveness of ELLA (see Figure 1). We then experiment on standard image classification benchmarks to exhibit the superiority of ELLA over competing baselines in aspects of both performance and scalability. We further show that ELLA can even scale up to modern architectures like vision transformers (ViTs) [11].

2 Background

Consider a learning problem on $\mathcal{D} = (\mathbf{X}, \mathbf{Y}) = \{(\mathbf{x}_i, \mathbf{y}_i)\}_{i=1}^N$, where $\mathbf{x}_i \in \mathcal{X}$ and $\mathbf{y}_i \in \mathbb{R}^C$ (e.g., regression) or $\{0, 1\}^C$ (e.g., classification) refer to observations and targets respectively. The advance in machine learning suggests using an NN $g_{\theta}(\cdot) : \mathcal{X} \rightarrow \mathbb{R}^C$ with parameters $\theta \in \mathbb{R}^P$ for data fitting. Despite well-performing, regularly trained NNs only capture the most likely interpretation for the data, thus miss the ability to reason about uncertainty and are prone to overfitting and overconfidence.

BNNs [37, 21, 44] characterize model uncertainty by probabilistic principle and can holistically represent all likely interpretations. Typically, BNNs impose a prior $p(\theta)$ on NN parameters and chase the Bayesian posterior $p(\theta|\mathcal{D}) = p(\mathcal{D}|\theta)p(\theta)/p(\mathcal{D})$ where $p(\mathcal{D}|\theta) = \prod_i p(\mathbf{y}_i|\mathbf{x}_i, \theta) = \prod_i p(\mathbf{y}_i|g_{\theta}(\mathbf{x}_i))$. Analytical estimation is usually intractable due to NNs’ high nonlinearity. Thereby, BNN methods usually find a surrogate of the true posterior $q(\theta) \approx p(\theta|\mathcal{D})$ via approximate inference methods like variational inference (VI) [1, 20, 36, 62, 29], Laplace approximation (LA) [38, 50], Markov chain Monte Carlo (MCMC) [55, 4, 63], particle-optimization based variational inference (POVI) [35], etc.

BNNs predict for new data \mathbf{x}_* by posterior predictive $p(\mathbf{y}|\mathbf{x}_*, \mathcal{D}) = \mathbb{E}_{p(\theta|\mathcal{D})}p(\mathbf{y}|\mathbf{x}_*, \theta) \approx \mathbb{E}_{q(\theta)}p(\mathbf{y}|\mathbf{x}_*, \theta) \approx \frac{1}{S} \sum_{s=1}^S p(\mathbf{y}|g_{\theta_s}(\mathbf{x}_*))$ where $\theta_s \sim q(\theta)$ are i.i.d. Monte Carlo (MC) samples.

2.1 Laplace Approximation and Its Linearized Variant

Typically, LA builds a Gaussian approximate posterior in the form of $q(\boldsymbol{\theta}) = \mathcal{N}(\boldsymbol{\theta}; \hat{\boldsymbol{\theta}}, \boldsymbol{\Sigma})$, where $\hat{\boldsymbol{\theta}}$ denotes the MAP solution, i.e., $\hat{\boldsymbol{\theta}} = \arg \max_{\boldsymbol{\theta}} \log p(\mathcal{D}|\boldsymbol{\theta}) + \log p(\boldsymbol{\theta})$, and $\boldsymbol{\Sigma}$ is the inversion of the Hessian of the negative log posterior w.r.t. parameters, i.e., $\boldsymbol{\Sigma}^{-1} = -\nabla_{\boldsymbol{\theta}\boldsymbol{\theta}}^2 (\log p(\mathcal{D}|\boldsymbol{\theta}) + \log p(\boldsymbol{\theta}))|_{\boldsymbol{\theta}=\hat{\boldsymbol{\theta}}}$. Without loss of generality, we base the following discussion on the isotropic Gaussian prior $p(\boldsymbol{\theta}) = \mathcal{N}(\boldsymbol{\theta}; \mathbf{0}, \sigma_0^2 \mathbf{I}_P)^1$, so $-\nabla_{\boldsymbol{\theta}\boldsymbol{\theta}}^2 \log p(\boldsymbol{\theta})|_{\boldsymbol{\theta}=\hat{\boldsymbol{\theta}}}$ equals to \mathbf{I}_P/σ_0^2 .

Due to the intractability of the Hessian for NNs with massive parameters, it is a common practice to use the symmetric positive and semi-definite (SPSD) GGN matrix as a workaround, i.e.,

$$\boldsymbol{\Sigma}^{-1} = \sum_i J_{\hat{\boldsymbol{\theta}}}(\mathbf{x}_i)^\top \Lambda(\mathbf{x}_i, \mathbf{y}_i) J_{\hat{\boldsymbol{\theta}}}(\mathbf{x}_i) + \mathbf{I}_P/\sigma_0^2, \quad (1)$$

where $J_{\hat{\boldsymbol{\theta}}}(\mathbf{x}) \triangleq \nabla_{\boldsymbol{\theta}} g_{\boldsymbol{\theta}}(\mathbf{x})|_{\boldsymbol{\theta}=\hat{\boldsymbol{\theta}}}$ and $\Lambda(\mathbf{x}, \mathbf{y}) \triangleq -\nabla_{\mathbf{g}\mathbf{g}}^2 \log p(\mathbf{y}|\mathbf{g})|_{\mathbf{g}=g_{\hat{\boldsymbol{\theta}}}(\mathbf{x})}$.

When concatenating $\{J_{\hat{\boldsymbol{\theta}}}(\mathbf{x}_i) \in \mathbb{R}^{C \times P}\}_{i=1}^N$ as a big matrix $\mathbf{J}_{\hat{\boldsymbol{\theta}}, \mathbf{X}} \in \mathbb{R}^{NC \times P}$ and organizing $\{\Lambda(\mathbf{x}_i, \mathbf{y}_i) \in \mathbb{R}^{C \times C}\}_{i=1}^N$ as a block-diagonal matrix $\boldsymbol{\Lambda}_{\mathbf{X}, \mathbf{Y}} \in \mathbb{R}^{NC \times NC}$, we have:

$$\boldsymbol{\Sigma} = \left[\mathbf{J}_{\hat{\boldsymbol{\theta}}, \mathbf{X}}^\top \boldsymbol{\Lambda}_{\mathbf{X}, \mathbf{Y}} \mathbf{J}_{\hat{\boldsymbol{\theta}}, \mathbf{X}} + \mathbf{I}_P/\sigma_0^2 \right]^{-1}. \quad (2)$$

Yet, LA suffers from underfitting [33]. This is probably because GGN approximation implicitly turns the original model $g_{\boldsymbol{\theta}}(\mathbf{x})$ into a linear one $g_{\hat{\boldsymbol{\theta}}}^{\text{lin}}(\mathbf{x}) = g_{\hat{\boldsymbol{\theta}}}(\mathbf{x}) + J_{\hat{\boldsymbol{\theta}}}(\mathbf{x})(\boldsymbol{\theta} - \hat{\boldsymbol{\theta}})$ but $g_{\boldsymbol{\theta}}(\mathbf{x})$ is still leveraged to make prediction. I.e., there exists a *shift* between posterior inference and prediction [22]. To mitigate this issue, a proposal is to predict with $g_{\hat{\boldsymbol{\theta}}}^{\text{lin}}(\mathbf{x})$, giving rise to linearized LA (LLA) [14, 28, 22].

LA and LLA nicely fit the *pretraining-finetuning* fashion in DL – they can be *post-hoc* applied to pretrained models where only the GGN matrices require to be estimated and further inverted. By LA and LLA, practitioners can adapt off-the-shelf high performing DNNs to BNNs easily.

LLA has revealed strong results on diverse UQ problems [14, 6, 7]. The Laplace library [6] further advances LLA’s applicability, and evidences LLA is competitive to popular alternatives [63, 32, 39].

Scalability issue The GGN matrix of size $P \times P$ is still unamenable in modern DL scenarios, so further approximations sparsifying it are always introduced. The diagonal and KFAC [40] approximations are commonly adopted ones [50, 62], where only a diagonal or block-diagonal structure of the original GGN matrix is preserved. An orthogonal tactic is to concern only a subspace of the high-dimensional parameter space (e.g., the parameter space of the last layer [30]) to reduce the scale of the GGN matrix. However, these strategies sacrifice the fidelity of the learning outcomes as the approximation errors in these cases can hardly be theoretically measured. To this end, we develop *accelerated Linearized Laplace Approximation (ELLA)* to push the limit of LLA in a more assurable way.

3 Methodology

In this section, we first revisit the relation of LLA to Gaussian processes (GPs) and Neural Tangent Kernels (NTKs) [24]. After that, we reveal how to accelerate LLA by kernel approximation. Based on these findings, we develop an efficient implementation of ELLA using the Nyström method [58].

3.1 The Gaussian Process View of LLA

Integrating $q(\boldsymbol{\theta}) = \mathcal{N}(\boldsymbol{\theta}; \hat{\boldsymbol{\theta}}, \boldsymbol{\Sigma})$ with the linear model $g_{\hat{\boldsymbol{\theta}}}^{\text{lin}}(\mathbf{x})$ actually gives rise to a function-space approximate posterior [14, 28, 22] in the form of $q(f) = \mathcal{GP}(f|g_{\hat{\boldsymbol{\theta}}}(\mathbf{x}), \kappa_{\text{LLA}}(\mathbf{x}, \mathbf{x}'))$ with

$$\kappa_{\text{LLA}}(\mathbf{x}, \mathbf{x}') \triangleq J_{\hat{\boldsymbol{\theta}}}(\mathbf{x}) \boldsymbol{\Sigma} J_{\hat{\boldsymbol{\theta}}}(\mathbf{x}')^\top. \quad (3)$$

By Woodbury matrix identity [60], we have:

$$\boldsymbol{\Sigma} = \left[\mathbf{J}_{\hat{\boldsymbol{\theta}}, \mathbf{X}}^\top \boldsymbol{\Lambda}_{\mathbf{X}, \mathbf{Y}} \mathbf{J}_{\hat{\boldsymbol{\theta}}, \mathbf{X}} + \mathbf{I}_P/\sigma_0^2 \right]^{-1} = \sigma_0^2 \left(\mathbf{I}_P - \mathbf{J}_{\hat{\boldsymbol{\theta}}, \mathbf{X}}^\top [\boldsymbol{\Lambda}_{\mathbf{X}, \mathbf{Y}}^{-1}/\sigma_0^2 + \mathbf{J}_{\hat{\boldsymbol{\theta}}, \mathbf{X}} \mathbf{J}_{\hat{\boldsymbol{\theta}}, \mathbf{X}}^\top]^{-1} \mathbf{J}_{\hat{\boldsymbol{\theta}}, \mathbf{X}} \right). \quad (4)$$

¹ \mathbf{I}_P refers to the identity matrix of size $P \times P$.

It follows that

$$\kappa_{\text{LLA}}(\mathbf{x}, \mathbf{x}') = \sigma_0^2 \left(\kappa_{\text{NTK}}(\mathbf{x}, \mathbf{x}') - \kappa_{\text{NTK}}(\mathbf{x}, \mathbf{X}) [\Lambda_{\mathbf{X}, \mathbf{Y}}^{-1} / \sigma_0^2 + \kappa_{\text{NTK}}(\mathbf{X}, \mathbf{X})]^{-1} \kappa_{\text{NTK}}(\mathbf{X}, \mathbf{x}') \right), \quad (5)$$

where $\kappa_{\text{NTK}}(\mathbf{x}, \mathbf{x}') \triangleq J_{\hat{\theta}}(\mathbf{x}) J_{\hat{\theta}}(\mathbf{x}')^\top$ denotes the neural tangent kernel (NTK) [24] corresponding to $g_{\hat{\theta}}(\mathbf{x})$. Note that $\kappa_{\text{NTK}}(\mathbf{x}, \mathbf{x}')$ is a *matrix-valued* kernel, with values in the space of $C \times C$ matrices.

The main challenge then turns into the computation and inversion of the gram matrix $\kappa_{\text{NTK}}(\mathbf{X}, \mathbf{X})$ of size $NC \times NC$. When either N or C is large, the estimation of κ_{LLA} still suffers from inefficiency issue. To address this, existing work [22] assumes independence among the C output dimensions to cast $q(f)$ into C independent GPs following [51], and randomly subsample $M \ll N$ data points to form a cheap substitute for the original gram matrix. Despite effective in some cases, these approximations are heuristic, lacking a clear theoretical foundation.

3.2 Scale Up LLA by Kernel Approximation

We show that if we can approximate $\kappa_{\text{NTK}}(\mathbf{x}, \mathbf{x}')$ with the inner product of some explicit $C \times K$ -dimensional representations of the data, i.e., $\kappa_{\text{NTK}}(\mathbf{x}, \mathbf{x}') \approx \varphi(\mathbf{x})\varphi(\mathbf{x}')^\top$ with $\varphi: \mathcal{X} \rightarrow \mathbb{R}^{C \times K}$, the scalability of the whole workflow can be unleashed.

Concretely, letting $\varphi_{\mathbf{X}} \in \mathbb{R}^{NC \times K}$ be the concatenation of $\{\varphi(\mathbf{x}_i) \in \mathbb{R}^{C \times K}\}_{i=1}^N$, we have (detailed derivation in Appendix A.2; see also [9])

$$\begin{aligned} \kappa_{\text{LLA}}(\mathbf{x}, \mathbf{x}') &\approx \sigma_0^2 \left(\varphi(\mathbf{x})\varphi(\mathbf{x}')^\top - \varphi(\mathbf{x})\varphi_{\mathbf{X}}^\top \left[\Lambda_{\mathbf{X}, \mathbf{Y}}^{-1} / \sigma_0^2 + \varphi_{\mathbf{X}}\varphi_{\mathbf{X}}^\top \right]^{-1} \varphi_{\mathbf{X}}\varphi(\mathbf{x}')^\top \right) \\ &= \varphi(\mathbf{x}) \underbrace{\left[\sum_i \varphi(\mathbf{x}_i)^\top \Lambda(\mathbf{x}_i, \mathbf{y}_i) \varphi(\mathbf{x}_i) + \mathbf{I}_K / \sigma_0^2 \right]^{-1}}_{\mathbf{G}} \varphi(\mathbf{x}')^\top \triangleq \kappa_{\text{ELLA}}(\mathbf{x}, \mathbf{x}'). \end{aligned} \quad (6)$$

The matrix $\mathbf{G} \in \mathbb{R}^{K \times K}$ possesses a similar formula to the Σ in the original κ_{LLA} in Equation (3), yet much smaller. Once having φ , it is only required to perform one forward pass of g and φ for each training data to estimate \mathbf{G} . When K is reasonably small, e.g., < 100 , it is cheap to invert \mathbf{G} .

3.3 Approximate NTKs via the Nyström Method

Typical kernel approximation means include Nyström method [45, 58] and random features-based methods [48, 49, 61, 43, 15, 9]. Given that the latter routinely relies on a relatively large number of random features to gain a faithful approximation (which means a large K), we suggest leveraging the Nyström method, which captures only several principal components of the kernel, to build φ .

To comfortably apply the Nyström method, we first rewrite $\kappa_{\text{NTK}}(\mathbf{x}, \mathbf{x}')$ as a *scalar-valued* kernel $\kappa_{\text{NTK}}((\mathbf{x}, i), (\mathbf{x}', i')) = J_{\hat{\theta}}(\mathbf{x}, i) J_{\hat{\theta}}(\mathbf{x}', i')^\top$ where $J_{\hat{\theta}}(\mathbf{x}, i) \triangleq \nabla_{\theta} [g_{\theta}(\mathbf{x})]^{(i)}|_{\theta=\hat{\theta}}: \mathcal{X} \times [C] \rightarrow \mathbb{R}^{1 \times P^2}$ computes the gradient of i -th output w.r.t. parameters.

By Mercer's theorem [42],

$$\kappa_{\text{NTK}}((\mathbf{x}, i), (\mathbf{x}', i')) = \sum_{k \geq 1} \mu_k \psi_k(\mathbf{x}, i) \psi_k(\mathbf{x}', i'), \quad (7)$$

where $\psi_k \in L^2(\mathcal{X} \times [C], q)^3$ refer to the eigenfunctions of the NTK w.r.t. some probability measure q with $\mu_k \geq 0$ as the associated eigenvalues. Based on this, the Nyström method discovers the top- K eigenvalues as well as the corresponding eigenfunctions for kernel approximation.

By definition, the eigenfunctions can represent the spectral information of the kernel:

$$\int \kappa_{\text{NTK}}((\mathbf{x}, i), (\mathbf{x}', i')) \psi_k(\mathbf{x}', i') q(\mathbf{x}', i') = \mu_k \psi_k(\mathbf{x}, i), \forall k \geq 1, \quad (8)$$

while being orthonormal under q :

$$\int \psi_k(\mathbf{x}, i) \psi_{k'}(\mathbf{x}, i) q(\mathbf{x}, i) = \mathbb{1}[k = k'], \forall k, k' \geq 1. \quad (9)$$

²We use superscript to index a multi-dimensional tensor and $[C]$ represents set of integers from 1 to C .

³ $L^2(q)$ denotes the space of square-integrable functions w.r.t. q .

In our case, $q(\mathbf{x}, i)$ can be factorized as the product of the data distribution and a uniform distribution over $\{1, \dots, C\}$, which can be trivially sampled from. The Nyström method draws M ($M \geq K$) i.i.d. samples $\tilde{\mathbf{X}} = \{(\mathbf{x}_1, i_1), \dots, (\mathbf{x}_M, i_M)\}$ from q to approximate the integration in Equation (8):

$$\frac{1}{M} \sum_{m=1}^M \kappa_{\text{NTK}}((\mathbf{x}, i), (\mathbf{x}_m, i_m)) \psi_k(\mathbf{x}_m, i_m) = \mu_k \psi_k(\mathbf{x}, i), \forall k \in [K]. \quad (10)$$

Applying this equation to these samples gives rise to:

$$\frac{1}{M} \sum_{m=1}^M \kappa_{\text{NTK}}((\mathbf{x}_{m'}, i_{m'}), (\mathbf{x}_m, i_m)) \psi_k(\mathbf{x}_m, i_m) = \mu_k \psi_k(\mathbf{x}_{m'}, i_{m'}), \forall k \in [K], m' \in [M], \quad (11)$$

then we arrive at

$$\frac{1}{M} \mathbf{K} \boldsymbol{\psi}_k \approx \mu_k \boldsymbol{\psi}_k, k \in [K], \quad (12)$$

where $\mathbf{K} = \mathbf{J}_{\hat{\boldsymbol{\theta}}, \tilde{\mathbf{X}}} \mathbf{J}_{\hat{\boldsymbol{\theta}}, \tilde{\mathbf{X}}}^\top$, with $\mathbf{J}_{\hat{\boldsymbol{\theta}}, \tilde{\mathbf{X}}} \in \mathbb{R}^{M \times P}$ as the concatenation of $\{J_{\hat{\boldsymbol{\theta}}}(\mathbf{x}_m, i_m) \in \mathbb{R}^{1 \times P}\}_{m=1}^M$, and $\boldsymbol{\psi}_k = [\psi_k(\mathbf{x}_1, i_1), \dots, \psi_k(\mathbf{x}_M, i_M)]^\top$. This implies a scaled eigendecomposition problem of \mathbf{K} .

We compute the top- K eigenvalues $\lambda_1, \dots, \lambda_K$ of matrix \mathbf{K} and record the corresponding *orthonormal* eigenvectors $\mathbf{u}_1, \dots, \mathbf{u}_K$. Given the constraint in Equation (9), it is easy to see that:

$$\mu_k \approx \frac{\lambda_k}{M}, \text{ and } \psi_k(\mathbf{x}_m, i_m) \approx \sqrt{M} \mathbf{u}_k^{(m)}, m \in [M]. \quad (13)$$

Combining Equation (13) and (10) yields the Nyström approximation of the top- K eigenfunctions:

$$\hat{\psi}_k(\mathbf{x}, i) = \frac{\sqrt{M}}{\lambda_k} \sum_{m=1}^M \mathbf{u}_k^{(m)} \kappa_{\text{NTK}}((\mathbf{x}, i), (\mathbf{x}_m, i_m)) = \frac{\sqrt{M}}{\lambda_k} J_{\hat{\boldsymbol{\theta}}}(\mathbf{x}, i) \mathbf{J}_{\hat{\boldsymbol{\theta}}, \tilde{\mathbf{X}}}^\top \mathbf{u}_k. \quad (14)$$

Then, the mapping φ which satisfied $\kappa_{\text{NTK}}(\mathbf{x}, \mathbf{x}') \approx \varphi(\mathbf{x}) \varphi(\mathbf{x}')^\top$ can be realized as:

$$[\varphi(\mathbf{x})]^{(i,k)} = \hat{\psi}_k(\mathbf{x}, i) \sqrt{\mu_k} = J_{\hat{\boldsymbol{\theta}}}(\mathbf{x}, i) \mathbf{J}_{\hat{\boldsymbol{\theta}}, \tilde{\mathbf{X}}}^\top \mathbf{u}_k / \sqrt{\lambda_k}, \quad (15)$$

$$\Rightarrow \varphi(\mathbf{x}) = [J_{\hat{\boldsymbol{\theta}}}(\mathbf{x}) \mathbf{v}_1, \dots, J_{\hat{\boldsymbol{\theta}}}(\mathbf{x}) \mathbf{v}_K] \text{ with } \mathbf{v}_k = \mathbf{J}_{\hat{\boldsymbol{\theta}}, \tilde{\mathbf{X}}}^\top \mathbf{u}_k / \sqrt{\lambda_k}. \quad (16)$$

Connection to sparse approximations of GPs A recent work [57] has shown that sparse variational Gaussian processes (SVGP) [53, 3] is algebraically equivalent to the Nyström approximation because the Evidence Lower BOund (ELBO) of the former encompasses the learning objective of the latter. That's to say, ELLA implicitly deploys a sparse approximation to the original GP predictive of LLA.

Discussion In this work, the developed Nyström approximation to NTKs is mainly used for accelerating the computation of the predictive covariance of LLA, while it can also be easily applied to future work on the practical application of NTKs.

3.4 Implementation

As shown, the estimation of φ on a data point \mathbf{x} degenerates as K JVPs, which can be accomplished by invoking *fwAD* for K times:

$$\begin{pmatrix} \hat{\boldsymbol{\theta}} \\ \mathbf{x}, \mathbf{v}_k \end{pmatrix} \xrightarrow{\text{forward}} \begin{pmatrix} g_{\hat{\boldsymbol{\theta}}}(\mathbf{x}) \\ J_{\hat{\boldsymbol{\theta}}}(\mathbf{x}) \mathbf{v}_k \end{pmatrix}, k \in [K], \quad (17)$$

where the model output $g_{\hat{\boldsymbol{\theta}}}(\mathbf{x})$ and the JVP $J_{\hat{\boldsymbol{\theta}}}(\mathbf{x}) \mathbf{v}_k$ are simultaneously computed in *one single forward pass*. Prevalent DL libraries like PyTorch [47] and Jax [2] have already been armed with the capability for *fwAD*. Algorithm 2 details the procedure of building φ in a PyTorch-like style.

With that, we can trivially compute the posterior $q(f)$ according to Equation (6), as detailed in Algorithm 1. The procedures for estimating \mathbf{G} and the posterior can both be batched for acceleration.

Computation overhead The estimation of φ involves M forward and backward passes of $g_{\hat{\boldsymbol{\theta}}}$ and the eigendecomposition of a matrix of size $M \times M$. After that, we only need to make $\{\mathbf{v}_k\}_{k=1}^K$ persistent, which amounts to *storing K more NN copies*. Estimating \mathbf{G}^{-1} requires scanning the training set once and inverting a matrix of $K \times K$, which is cheap. The evaluation of $q(f)$ embodies that of φ , i.e., performing K forward passes under the scope of *fwAD*. This is similar to other BNNs that perform S forward passes with different MC parameter samples to estimate the posterior predictive.

Algorithm 1: Build the LLA posterior.

```

#  $g_{\hat{\theta}}$ : NN pre-trained by MAP;  $(\mathbf{X}, \mathbf{Y})$ :
# training set;  $C$ : number of classes
#  $M, K, \sigma_0^2$ : hyper-parameters
def estimate_G( $\varphi, \mathbf{X}, \mathbf{Y}, K, \sigma_0^2$ ):
     $\mathbf{G} = \text{zeros}(K, K)$ 
    for  $(\mathbf{x}, \mathbf{y})$  in  $(\mathbf{X}, \mathbf{Y})$ :
         $g_{\mathbf{x}}, \varphi_{\mathbf{x}} = \varphi(\mathbf{x})$ 
         $\Lambda_{\mathbf{x}, \mathbf{y}} = \text{hessian}(\text{nll}(g_{\mathbf{x}}, \mathbf{y}), g_{\mathbf{x}})$ 
         $\mathbf{G} += \varphi_{\mathbf{x}}^{\top} \Lambda_{\mathbf{x}, \mathbf{y}} \varphi_{\mathbf{x}}$ 
    return  $\mathbf{G} + \text{eye}(K) / \sigma_0^2$ 
def _q_f( $\varphi, \mathbf{G}^{-1}, \mathbf{x}$ )
     $g_{\mathbf{x}}, \varphi_{\mathbf{x}} = \varphi(\mathbf{x})$ 
     $\kappa_{\mathbf{x}, \mathbf{x}} = \varphi_{\mathbf{x}} \mathbf{G}^{-1} \varphi_{\mathbf{x}}^{\top}$ 
    return  $\mathcal{N}(g_{\mathbf{x}}, \kappa_{\mathbf{x}, \mathbf{x}})$ 
 $\varphi = \text{build}_{\varphi}(g_{\hat{\theta}}, \mathbf{X}, C, M, K)$ 
 $\mathbf{G}^{-1} = \text{inv}(\text{estimate}_{\mathbf{G}}(\varphi, \mathbf{X}, \mathbf{Y}, K, \sigma_0^2))$ 
q_f = partial(_q_f,  $\varphi, \mathbf{G}^{-1}$ )

```

Algorithm 2: Build φ .

```

def build_{\varphi}( $g_{\hat{\theta}}, \mathbf{X}, C, M, K$ ):
    def _{\varphi}( $g_{\hat{\theta}}, C, \{\mathbf{v}_k\}_{k=1}^K, \mathbf{x}$ ):
         $\varphi_{\mathbf{x}} = \text{zeros}(C, K)$ 
        for  $k$  in range( $K$ ):
            with fwAD.enable():
                 $g_{\mathbf{x}}, jvp = g_{(\hat{\theta}, \mathbf{v}_k)}(\mathbf{x})$ 
                 $\varphi_{\mathbf{x}}[:, k] = jvp$ 
        return  $g_{\mathbf{x}}, \varphi_{\mathbf{x}}$ 
     $\mathbf{J}_{\hat{\theta}, \tilde{\mathbf{x}}} = \text{zeros}(M, \text{dim}(\hat{\theta}))$ 
    for  $m$  in range( $M$ ):
         $\mathbf{x}_m = \text{uniform\_sample}(\mathbf{X})$ 
         $i_m = \text{uniform\_sample}(C)$ 
         $\mathbf{J}_{\hat{\theta}, \tilde{\mathbf{x}}}[m] = \text{grad}(g_{\hat{\theta}}(\mathbf{x}_m)[i_m], \hat{\theta})$ 
         $\{\lambda_k, \mathbf{u}_k\}_{k=1}^K = \text{eig}(\mathbf{J}_{\hat{\theta}, \tilde{\mathbf{x}}} \mathbf{J}_{\hat{\theta}, \tilde{\mathbf{x}}}^{\top}, \text{top} = K)$ 
    for  $k$  in range( $K$ ):
         $\mathbf{v}_k = \mathbf{J}_{\hat{\theta}, \tilde{\mathbf{x}}}^{\top} \mathbf{u}_k / \sqrt{\lambda_k}$ 
    return partial(_{\varphi},  $g_{\hat{\theta}}, C, \{\mathbf{v}_k\}_{k=1}^K$ )

```

4 Theoretical Analysis

In this section, we theoretically analyze the approximation error of $\kappa_{\text{ELLA}}(\mathbf{x}, \mathbf{x}')$ to $\kappa_{\text{LLA}}(\mathbf{x}, \mathbf{x}')$.

To reduce unnecessary complexity, this section assumes using $M = K$ i.i.d. MC samples when performing the Nyström method. Then, κ_{ELLA} can be reformulated as (details deferred to Appendix A.3)

$$\kappa_{\text{ELLA}}(\mathbf{x}, \mathbf{x}') = \mathbf{J}_{\hat{\theta}}(\mathbf{x}) \underbrace{\mathbf{J}_{\hat{\theta}, \tilde{\mathbf{x}}}^{\top} \left[\mathbf{J}_{\hat{\theta}, \tilde{\mathbf{x}}} \mathbf{J}_{\hat{\theta}, \mathbf{X}}^{\top} \Lambda_{\mathbf{X}, \mathbf{Y}} \mathbf{J}_{\hat{\theta}, \mathbf{X}} \mathbf{J}_{\hat{\theta}, \tilde{\mathbf{x}}}^{\top} + \mathbf{J}_{\hat{\theta}, \tilde{\mathbf{x}}} \mathbf{J}_{\hat{\theta}, \tilde{\mathbf{x}}}^{\top} / \sigma_0^2 \right]^{-1} \mathbf{J}_{\hat{\theta}, \tilde{\mathbf{x}}} \mathbf{J}_{\hat{\theta}}(\mathbf{x}')^{\top}}_{\Sigma'} \quad (18)$$

Thereby, the gap between $\kappa_{\text{ELLA}}(\mathbf{x}, \mathbf{x}')$ and $\kappa_{\text{LLA}}(\mathbf{x}, \mathbf{x}')$ can be upper bounded by $\mathcal{E} = \|\Sigma' - \Sigma\|$, where $\|\cdot\|$ represents the matrix 2-norm (i.e., the spectral norm). In typical cases, $P \gg M$, thus with high probability $\mathbf{K} = \mathbf{J}_{\hat{\theta}, \tilde{\mathbf{x}}} \mathbf{J}_{\hat{\theta}, \tilde{\mathbf{x}}}^{\top} \succ 0$. We present an upper bound of \mathcal{E} as follows.

Theorem 1 (Proof in Appendix A.4). *Let c_{Λ} be a finite constant associated with Λ , and \mathcal{E}' the error of Nyström approximation $\|\mathbf{J}_{\hat{\theta}, \mathbf{X}} \mathbf{J}_{\hat{\theta}, \tilde{\mathbf{x}}}^{\top} (\mathbf{J}_{\hat{\theta}, \tilde{\mathbf{x}}} \mathbf{J}_{\hat{\theta}, \tilde{\mathbf{x}}}^{\top})^{-1} \mathbf{J}_{\hat{\theta}, \tilde{\mathbf{x}}} \mathbf{J}_{\hat{\theta}, \mathbf{X}}^{\top} - \mathbf{J}_{\hat{\theta}, \mathbf{X}} \mathbf{J}_{\hat{\theta}, \mathbf{X}}^{\top}\|$. It holds that*

$$\mathcal{E} \leq \sigma_0^4 c_{\Lambda} \mathcal{E}' + \sigma_0^2.$$

\mathcal{E}' has been extensively analyzed by pioneering work [12, 5, 26], and we simply adapt the results developed by Drineas and Mahoney [12] to our case. We denote the maximum diagonal entry and the $M + 1$ -th largest eigenvalue of $\mathbf{J}_{\hat{\theta}, \mathbf{X}} \mathbf{J}_{\hat{\theta}, \mathbf{X}}^{\top}$ by c_{κ} and $\tilde{\lambda}_{M+1}$ respectively.

Theorem 2 (Error bound of Nyström approximation). *With probability at least $1 - \delta$, it holds that:*

$$\mathcal{E}' \leq \tilde{\lambda}_{M+1} + \frac{NC}{\sqrt{M}} c_{\kappa} (2 + \log \frac{1}{\delta}).$$

Plugging this back to \mathcal{E} , we arrive at the corollary below.

Corollary 1. *With probability at least $1 - \delta$, the following bound exists:*

$$\mathcal{E} \leq \sigma_0^4 c_{\Lambda} (\tilde{\lambda}_{M+1} + \frac{NC}{\sqrt{M}} c_{\kappa} (2 + \log \frac{1}{\delta})) + \sigma_0^2.$$

As desired, the upper bound of \mathcal{E} decreases along with the growing of the number of MC samples M .

5 Experiments

We first discuss how to specify the hyperparameters of ELLA, then expose an interesting finding. After that, we compare ELLA to competing baselines to evidence its merits in efficacy and scalability.

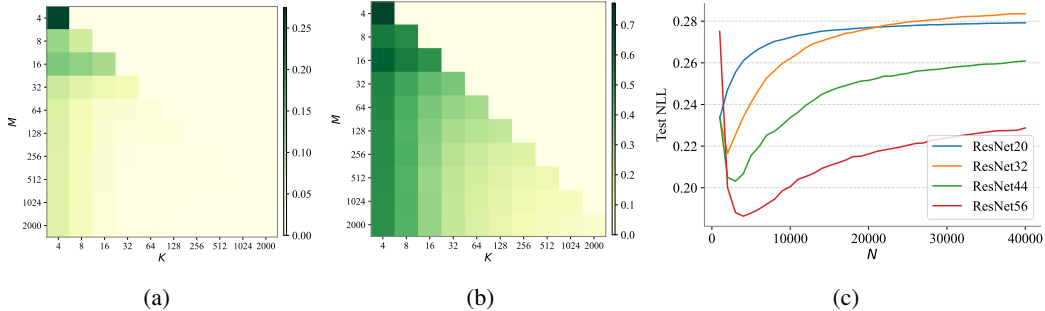


Figure 2: (a)-(b): The approximation errors $\epsilon_{\text{Nyström}}$ and ϵ_{ELLA} vary w.r.t. M and K ($M \geq K$). (c): The test NLL of ELLA on CIFAR-10 varies w.r.t. the number of training data N .

5.1 Specification of Hyperparameters

Given an NN $g_{\hat{\theta}}$ pretrained by MAP, we need to specify the prior variance σ_0^2 , the number of MC samples in Nyström method M , and the number of remaining eigenpairs K before applying ELLA. We simply set σ_0^2 to $\frac{1}{N^\gamma}$ with γ as the weight decay coefficient used for pretraining according to [10].

We perform an empirical study to inspect how M and K affect the quality of the Nyström approximation and the ELLA GP covariance. We take 2000 MNIST images as training set \mathbf{X} , and 256 others as validation set \mathbf{X}_{val} . The architecture contains 2 convolutions and a linear head. Batch normalization [23] and ReLU activation are used. The number of parameters P is 29,034. Larger architectures or larger \mathbf{X} will render the exact evaluation of κ_{LLA} unapproachable. We quantify the approximation error of the Nyström method by $\epsilon_{\text{Nyström}} \triangleq \|\mathbf{J}_{\hat{\theta}, \mathbf{X}} \mathbf{J}_{\hat{\theta}, \bar{\mathbf{X}}}^\top (\mathbf{J}_{\hat{\theta}, \bar{\mathbf{X}}} \mathbf{J}_{\hat{\theta}, \bar{\mathbf{X}}}^\top)^{-1} \mathbf{J}_{\hat{\theta}, \bar{\mathbf{X}}} \mathbf{J}_{\hat{\theta}, \mathbf{X}}^\top - \mathbf{J}_{\hat{\theta}, \mathbf{X}} \mathbf{J}_{\hat{\theta}, \mathbf{X}}^\top\| / \|\mathbf{J}_{\hat{\theta}, \mathbf{X}} \mathbf{J}_{\hat{\theta}, \mathbf{X}}^\top\|$, and that from κ_{ELLA} to κ_{LLA} by $\epsilon_{\text{ELLA}} \triangleq \frac{1}{|\mathbf{X}_{\text{val}}|} \sum_{\mathbf{x} \in \mathbf{X}_{\text{val}}} \|\kappa_{\text{ELLA}}(\mathbf{x}, \mathbf{x}) - \kappa_{\text{LLA}}(\mathbf{x}, \mathbf{x})\| / \|\kappa_{\text{LLA}}(\mathbf{x}, \mathbf{x})\|$. We vary M from 4 to 2000 and K from 4 to M , and report the approximation errors in Figure 2 (a)-(b). We notice that 1) the larger K the better; 2) when fixing K , $\epsilon_{\text{Nyström}}$ and ϵ_{ELLA} decay as M grows; 3) $\epsilon_{\text{Nyström}}$ decays more rapidly than ϵ_{ELLA} , echoing Theorem 1. Given that ELLA needs to store K vectors of size P , small K is desired for efficiency. $K \in [16, 32]$ seems to be a reasonable choice given Figure 2. Besides, Appendix C.1 includes a direct study on how the test NLL of ELLA varies w.r.t. M and K on CIFAR-10 [31] benchmark. Given these results, we set $M = 2000$ and $K = 20$ in the following experiments unless otherwise stated.

ELLA (or LLA) finds a GP posterior, so predicts with a variant of the aforementioned posterior predictive, formulated as $p(\mathbf{y}|\mathbf{x}_*, \mathcal{D}) = \mathbb{E}_{p(f|\mathcal{D})} p(\mathbf{y}|f(\mathbf{x}_*)) \approx \mathbb{E}_{q(f)} p(\mathbf{y}|f(\mathbf{x}_*)) = \mathbb{E}_{\mathbf{f} \sim \mathcal{N}(g_{\hat{\theta}}(\mathbf{x}_*), \kappa_{\text{ELLA}}(\mathbf{x}_*, \mathbf{x}_*))} p(\mathbf{y}|\mathbf{f})$. In classification tasks, we use 512 MC samples to approximate the last expectation and it is cheap.

5.2 The Overfitting Issue of LLA

Reinspecting Equation (1) and (6), we see, with more training data involved, the covariance in LA, LLA, and ELLA shrinks and the uncertainty dissipates. However, under ubiquitous model misspecification [41], *should the uncertainty vanish that fast?* We perform a study with ResNets [18] on CIFAR-10 to seek an answer. Concretely, we randomly subsample N data from the training set of CIFAR-10, and fit ELLA on them. We depict the test negative log-likelihood (NLL), accuracy, and expected calibration error (ECE) [17] of the deployed ELLA in Figure 2 (c) and Appendix C.2. We also provide the corresponding results of LLA*⁴ in Appendix C.3. The *V-shape* NLL curves across settings reflect the *overfitting* issue of ELLA and LLA* (or more generally, LLA). Figure 7 also shows that tuning the prior precision w.r.t. marginal likelihood can alleviate the overfitting of LLA* to some extent, which may be the reason why such an issue has not been reported by previous works. But also of note that tuning the prior precision cannot fully eliminate overfitting.

To address the overfitting issue, we advocate *performing early stop when fitting ELLA/LLA on big data*. Specifically, when iterating over the training data to estimate \mathbf{G} (see Equation (6)), we

⁴We experiment on LLA* here due to its higher efficiency than LLA-KFAC and LLA-Diag. LLA* is the default option in the Laplace library [6].

Table 1: Comparison on test accuracy (%) \uparrow , NLL \downarrow , and ECE \downarrow on CIFAR-10. We report the average results over 5 random runs. As the accuracy values of most methods are close, we do not highlight the best.

Method	ResNet-20			ResNet-32			ResNet-44			ResNet-56		
	Acc.	NLL	ECE	Acc.	NLL	ECE	Acc.	NLL	ECE	Acc.	NLL	ECE
<i>ELLA</i>	92.5	0.233	0.009	93.5	0.215	0.008	93.9	0.204	0.007	94.4	0.187	0.007
<i>MAP</i>	92.6	0.282	0.039	93.5	0.292	0.041	94.0	0.275	0.039	94.4	0.252	0.037
<i>MFVI-BF</i>	92.7	0.231	0.016	93.5	0.222	0.020	93.9	0.206	0.018	94.4	0.188	0.016
<i>LLA*</i>	92.6	0.269	0.034	93.5	0.259	0.033	94.0	0.237	0.028	94.4	0.213	0.022
<i>LLA*-KFAC</i>	92.6	0.271	0.035	93.5	0.260	0.033	94.0	0.232	0.028	94.4	0.202	0.024
<i>LLA-Diag</i>	92.2	0.728	0.404	92.7	0.755	0.430	92.8	0.778	0.445	92.9	0.843	0.480
<i>LLA-KFAC</i>	92.0	0.852	0.467	91.8	1.027	0.547	91.4	1.091	0.566	89.8	1.174	0.579

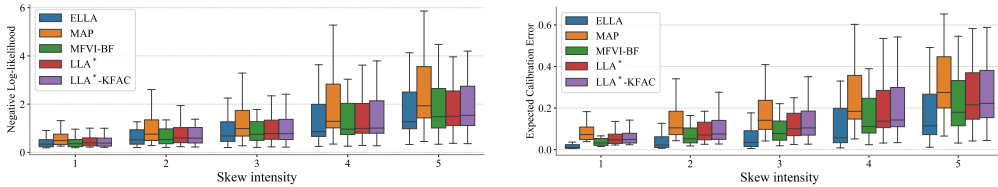


Figure 3: NLL (Left) and ECE (Right) on CIFAR-10 corruptions for models trained with ResNet-56 architecture. Each box corresponds to a summary of the results across 19 types of skew.

continuously record the NLL of the current ELLA posterior on some validation data, and stop when there is a trend of overfitting. If we cannot access a validation set easily, we can apply strong data augmentation to some training data to form a substitute of the validation set. Compared to tuning the prior, early stopping also helps reduce the time cost of processing big data (e.g., ImageNet [8]).

5.3 Illustrative Regression

We build a regression problem with $N = 16$ samples from $y = \sin 2x + \epsilon$, $\epsilon \sim \mathcal{N}(0, 0.2)$ as shown in Figure 1. The model is an MLP with 3 hidden layers and \tanh activations, and we pretrain it by MAP for 1000 iterations. For ELLA, we set $M = 16$ and $K = 5$ for efficiency. Unless stated otherwise, we use the interfaces of Laplace [6] to implement LLA, LLA-KFAC, LLA-Diag, and LLA*. The hyperparameters of the competitors are *equivalent* to those of ELLA except for some dedicated ones like M and K . It is clear that ELLA delivers a closer approximation to LLA than LLA-Diag and LLA*. We further quantify the quality of the predictive distributions produced by these approximate LLA methods using certain metrics. Considering that in this case, the predictive distribution for one test datum is a Gaussian distribution, we use the KL divergence between the Gaussians yielded by the approximate LLA method and vanilla LLA as a proxy of the approximation error (averaged over a set of test points). The results are reported in Appendix C.4. As shown, LLA-KFAC comes pretty close to LLA. Yet, LLA seems to *underestimate* in-between uncertainty in this setting, so ELLA seems to be a more reliable (instead of more accurate) approximation than LLA-KFAC. We also highlight the higher scalability of ELLA than LLA-KFAC (see Figure 4(c)), which reflects that ELLA can strike a good trade-off between efficacy and efficiency.

5.4 CIFAR-10 Classification

Then, we evaluate ELLA on CIFAR-10 benchmark using ResNet architectures [18]. We obtain pretrained MAP models from the open source community. Apart from MAP, LLA*, LLA-Diag, LLA-KFAC, we further introduce last-layer LLA with KFAC approximation (LLA*-KFAC) and mean-field VI via Bayesian finetuning [10] (MFVI-BF)⁵ as baselines. LLA cannot be directly applied as the GGN matrices are huge. These methods all locate in the family of Gaussian approximate posteriors and are all *post-hoc* applied to the pretrained models, so the comparisons will be fair. Regarding the setups, we use $M = 2000$ and $K = 20$ for ELLA,⁶ we use 20 MC samples to estimate

⁵Flipout [56] trick is deployed for variance-reduced gradient estimation.

⁶Storing 2000 vectors of size P is costly, so we trade time for memory and compute them whenever needed.

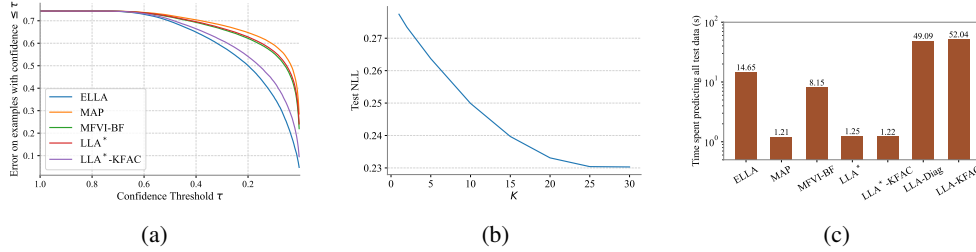


Figure 4: (a) Error versus confidence plots for methods trained on CIFAR-10 and tested on CIFAR-10+SVHN. (b) Test NLL of ELLA varies w.r.t. K on CIFAR-10. (c) Comparison on the wall-clock time used for predicting all CIFAR-10 test data (measured on an NVIDIA A40 GPU). The results are obtained with ResNet-20 architecture.

Table 2: Comparison on test accuracy (%) \uparrow , NLL \downarrow , and ECE \downarrow on ImageNet. We report the average results over 3 random runs.

Method	ResNet-18			ResNet-34			ResNet-50		
	Acc.	NLL	ECE	Acc.	NLL	ECE	Acc.	NLL	ECE
<i>ELLA</i>	69.8	1.243	0.015	73.3	1.072	0.018	76.2	0.948	0.018
<i>MAP</i>	69.8	1.247	0.026	73.3	1.081	0.035	76.2	0.962	0.037
<i>MFVI-BF</i>	70.3	1.218	0.042	73.7	1.043	0.033	76.1	0.945	0.030

the posterior predictive of MFVI-BF (as it incurs 20 NN forward passes), and use 512 ones for the other methods as stated. We have enabled *the tuning of the prior precision* for all LLA baselines, but not for ELLA.

We present the comparison on test accuracy, NLL, and ECE in Table 1. As shown, ELLA exhibits superior NLL and ECE across settings. MFVI-BF also gives good NLL. LLA* and LLA*-KFAC can improve the uncertainty and calibration of MAP, yet underperforming ELLA. LLA-Diag and LLA-KFAC fail for unclear reasons (also reported by [9]), we thus exclude them from the following studies.

We then examine the models on the widely used out-of-distribution (OOD) generalization/robustness benchmark CIFAR-10 corruptions [19] and report the results in Figure 3 and Appendix C.5. It is prominent that ELLA surpasses the baselines in aspects of NLL and ECE at various levels of skew, implying its ability to make conservative predictions for OOD inputs.

We further evaluate the models on the combination of the CIFAR-10 test data and the OOD SVHN test data. The predictions on SVHN are all regarded as wrong due to label shift. We plot the average error rate of the samples with $\leq \tau$ ($\tau \in [0, 1]$) confidence in Figure 4 (a). As shown, ELLA makes less mistakes than the baselines under various confidence thresholds. Figure 4 (b) displays how K impacts the test NLL. We see that $K \in [20, 30]$ can already lead to good performance, reflecting the efficiency of ELLA. Another benefit of ELLA is that with it, we can actively control the performance vs. cost trade-off. Figure 4 (c) shows the comparison on the time used for predicting all CIFAR-10 test data. We note that ELLA is slightly slower than MFVI and substantially faster than *non-last-layer* LLA methods.

5.5 ImageNet Classification

We apply ELLA to ImageNet classification [8] to demonstrate its scalability. The experiment settings are identical with those for CIFAR-10. We observe that all LLA methods implemented with `Laplace` would cause out-of-memory (OOM) errors or suffer from very long fitting procedures, thus take only MAP and MFVI-BF as baselines. Table 2 presents the comparison on test accuracy, NLL, and ECE with ResNet architectures. We see that ELLA maintains its superiority in ECE while MFVI-BF can induce higher accuracy and lower NLL. This may be attributed to that the pretrained MAP model lies at a sharp maxima of the true posterior so it is necessary to properly adjust the mean of the Gaussian approximate posterior.

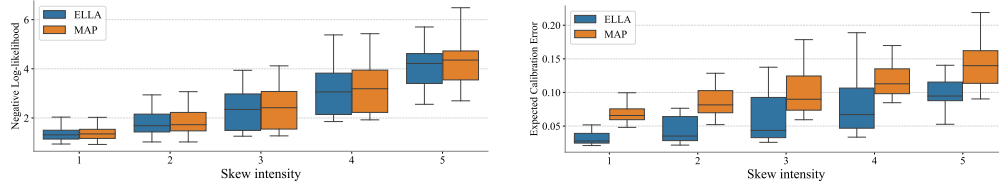


Figure 5: NLL (Left) and ECE (Right) on ImageNet corruptions for models trained with ViT-B architecture. Each box corresponds to a summary of the results across 19 types of skew.

We lastly apply ELLA to ViT-B [11]. We compare ELLA to MAP in Table 3 as all other baselines incur OOM errors or crushingly long running time. As shown, ELLA beats MAP in multiple aspects. Figure 5 shows the results of ELLA and MAP on ImageNet corruptions [19]. They are consistent with those for CIFAR-10 corruptions. We reveal by this experiment that ELLA can be a more applicable and scalable method than most of existing BNNs.

Table 3: Comparison on test accuracy (%) \uparrow , NLL \downarrow , and ECE \downarrow on ImageNet with ViT-B architecture.

Method	Acc.	NLL	ECE
<i>ELLA</i>	81.6	0.695	0.022
<i>MAP</i>	81.5	0.700	0.039

6 Related Work

LA [38, 50, 14, 30, 22, 6, 7] locally approximates the Bayesian posterior with a Gaussian distribution, analogous to VI with Gaussian variationals [16, 1, 36, 52, 46] and SWAG [39]. LA can be applied to pretrained models effortlessly while the acquired posteriors are potentially restrictive (see Section 5.5). VI enjoys higher flexibility yet relies on costly training; BayesAdapter [10] seems to be a remedy to the issue but its accessibility is still lower than LA. SWAG stores a series of SGD iterates to heuristically construct an approximate posterior and is empirically weaker than LA/LLA [6].

Though more expressive approaches like deep ensembles [32] and MCMC [55, 4, 63] can explicitly explore diverse posterior modes, they face limitations in efficiency and scalability. What’s more, it has been shown that LA/LLA can perform on par with or better than deep ensembles and cyclical MCMC on multiple benchmarks [6]. This may be attributed to the un-identified, complicated relationships between the parameters space and the function space of DNNs [59]. Also of note that LA can embrace deep ensembles to capture multiple posterior modes [13].

[9] introduces a general kernel approximation technique using neural networks. By contrast, we focus on leveraging kernel approximation to accelerate Laplace approximation. Thus, the focus of the two works is distinct. Indeed, this work shares a similar idea with the Sec 4.3 in [9] that LLA can be accelerated by kernel approximation. But, except for such an idea, this work differentiates from [9] in aspects like motivations, techniques, implementations, theoretical backgrounds, and applications. Our implementation, theoretical analysis, and some empirical findings are all novel.

7 Conclusion

This paper proposes ELLA, a simple, effective, and reliable approach for Bayesian deep learning. ELLA addresses the unreliability issues of existing approximations to LLA and is implemented based on Nyström method. We offer theoretical guarantees for ELLA and perform extensive studies to testify its efficacy and scalability. ELLA currently accounts for only the predictive, and extending it to estimate model evidence for model selection [38] deserves future investigation. Using model evidence to select the number of remaining eigenpairs K for ELLA is also viable.

Acknowledgments and Disclosure of Funding

This work was supported by NSF of China Projects (Nos. 62061136001, 62076145, 62106121, U19B2034, U1811461, U19A2081, 6197222); Beijing NSF Project (No. JQ19016); a grant from Tsinghua Institute for Guo Qiang; and the High Performance Computing Center, Tsinghua University. J.Z was also supported by the XPlorer Prize

References

- [1] Charles Blundell, Julien Cornebise, Koray Kavukcuoglu, and Daan Wierstra. Weight uncertainty in neural network. In *International Conference on Machine Learning*, pages 1613–1622, 2015.
- [2] James Bradbury, Roy Frostig, Peter Hawkins, Matthew James Johnson, Chris Leary, Dougal Maclaurin, George Necula, Adam Paszke, Jake VanderPlas, Skye Wanderman-Milne, and Qiao Zhang. JAX: composable transformations of Python+NumPy programs, 2018.
- [3] David Burt, Carl Edward Rasmussen, and Mark Van Der Wilk. Rates of convergence for sparse variational gaussian process regression. In *International Conference on Machine Learning*, pages 862–871. PMLR, 2019.
- [4] Tianqi Chen, Emily Fox, and Carlos Guestrin. Stochastic gradient hamiltonian monte carlo. In *International Conference on Machine Learning*, pages 1683–1691. PMLR, 2014.
- [5] Corinna Cortes, Mehryar Mohri, and Ameet Talwalkar. On the impact of kernel approximation on learning accuracy. In *International Conference on Artificial Intelligence and Statistics*, pages 113–120. JMLR Workshop and Conference Proceedings, 2010.
- [6] Erik Daxberger, Agustinus Kristiadi, Alexander Immer, Runa Eschenhagen, Matthias Bauer, and Philipp Hennig. Laplace redux-effortless bayesian deep learning. *Advances in Neural Information Processing Systems*, 34, 2021.
- [7] Erik Daxberger, Eric Nalisnick, James U Allingham, Javier Antorán, and José Miguel Hernández-Lobato. Bayesian deep learning via subnetwork inference. In *International Conference on Machine Learning*, pages 2510–2521. PMLR, 2021.
- [8] J. Deng, W. Dong, R. Socher, L.-J. Li, K. Li, and L. Fei-Fei. ImageNet: A Large-Scale Hierarchical Image Database. In *Proceedings of the IEEE Conference on Computer Vision and Pattern Recognition*, 2009.
- [9] Zhijie Deng, Jiaxin Shi, and Jun Zhu. Neuralef: Deconstructing kernels by deep neural networks. *arXiv preprint arXiv:2205.00165*, 2022.
- [10] Zhijie Deng, Hao Zhang, Xiao Yang, Yinpeng Dong, and Jun Zhu. Bayesadapter: Being bayesian, inexpensively and reliably, via bayesian fine-tuning. *arXiv preprint arXiv:2010.01979*, 2020.
- [11] Alexey Dosovitskiy, Lucas Beyer, Alexander Kolesnikov, Dirk Weissenborn, Xiaohua Zhai, Thomas Unterthiner, Mostafa Dehghani, Matthias Minderer, Georg Heigold, Sylvain Gelly, et al. An image is worth 16x16 words: Transformers for image recognition at scale. In *International Conference on Learning Representations*, 2020.
- [12] Petros Drineas, Michael W Mahoney, and Nello Cristianini. On the nyström method for approximating a gram matrix for improved kernel-based learning. *Journal of Machine Learning Research*, 6(12), 2005.
- [13] Runa Eschenhagen, Erik Daxberger, Philipp Hennig, and Agustinus Kristiadi. Mixtures of laplace approximations for improved post-hoc uncertainty in deep learning. *arXiv preprint arXiv:2111.03577*, 2021.
- [14] Andrew YK Foong, Yingzhen Li, José Miguel Hernández-Lobato, and Richard E Turner. ‘in-between’ uncertainty in bayesian neural networks. *arXiv preprint arXiv:1906.11537*, 2019.
- [15] Deena P Francis and Kumudha Raimond. Major advancements in kernel function approximation. *Artificial Intelligence Review*, 54(2):843–876, 2021.
- [16] Alex Graves. Practical variational inference for neural networks. In *Advances in Neural Information Processing Systems*, pages 2348–2356, 2011.
- [17] Chuan Guo, Geoff Pleiss, Yu Sun, and Kilian Q Weinberger. On calibration of modern neural networks. *arXiv preprint arXiv:1706.04599*, 2017.
- [18] Kaiming He, Xiangyu Zhang, Shaoqing Ren, and Jian Sun. Deep residual learning for image recognition. In *Proceedings of the IEEE Conference on Computer Vision and Pattern Recognition*, pages 770–778, 2016.
- [19] Dan Hendrycks and Thomas Dietterich. Benchmarking neural network robustness to common corruptions and perturbations. *arXiv preprint arXiv:1903.12261*, 2019.
- [20] José Miguel Hernández-Lobato and Ryan Adams. Probabilistic backpropagation for scalable learning of Bayesian neural networks. In *International Conference on Machine Learning*, pages 1861–1869, 2015.
- [21] Geoffrey Hinton and Drew Van Camp. Keeping neural networks simple by minimizing the description length of the weights. In *ACM Conference on Computational Learning Theory*, 1993.
- [22] Alexander Immer, Maciej Korzepa, and Matthias Bauer. Improving predictions of bayesian neural nets via local linearization. In *International Conference on Artificial Intelligence and Statistics*, pages 703–711. PMLR, 2021.

- [23] Sergey Ioffe and Christian Szegedy. Batch normalization: Accelerating deep network training by reducing internal covariate shift. In *International Conference on Machine Learning*, pages 448–456. PMLR, 2015.
- [24] Arthur Jacot, Franck Gabriel, and Clément Hongler. Neural tangent kernel: Convergence and generalization in neural networks. *arXiv preprint arXiv:1806.07572*, 2018.
- [25] Huisu Jang and Jaewook Lee. An empirical study on modeling and prediction of bitcoin prices with bayesian neural networks based on blockchain information. *Ieee Access*, 6:5427–5437, 2017.
- [26] Rong Jin, Tianbao Yang, Mehrdad Mahdavi, Yu-Feng Li, and Zhi-Hua Zhou. Improved bounds for the nyström method with application to kernel classification. *IEEE Transactions on Information Theory*, 59(10):6939–6949, 2013.
- [27] Alex Kendall and Yarin Gal. What uncertainties do we need in Bayesian deep learning for computer vision? In *Advances in Neural Information Processing Systems*, pages 5574–5584, 2017.
- [28] Mohammad Emtiyaz Khan, Alexander Immer, Ehsan Abedi, and Maciej Korzepa. Approximate inference turns deep networks into gaussian processes. *arXiv preprint arXiv:1906.01930*, 2019.
- [29] Mohammad Emtiyaz Khan, Didrik Nielsen, Voot Tangkaratt, Wu Lin, Yarin Gal, and Akash Srivastava. Fast and scalable Bayesian deep learning by weight-perturbation in adam. In *International Conference on Machine Learning*, pages 2616–2625, 2018.
- [30] Agustinus Kristiadi, Matthias Hein, and Philipp Hennig. Being bayesian, even just a bit, fixes overconfidence in relu networks. *arXiv preprint arXiv:2002.10118*, 2020.
- [31] Alex Krizhevsky, Geoffrey Hinton, et al. Learning multiple layers of features from tiny images. 2009.
- [32] Balaji Lakshminarayanan, Alexander Pritzel, and Charles Blundell. Simple and scalable predictive uncertainty estimation using deep ensembles. In *Advances in Neural Information Processing Systems*, pages 6402–6413, 2017.
- [33] Neil David Lawrence. *Variational inference in probabilistic models*. PhD thesis, Citeseer, 2001.
- [34] Christian Leibig, Vaneeda Allken, Murat Seçkin Ayhan, Philipp Berens, and Siegfried Wahl. Leveraging uncertainty information from deep neural networks for disease detection. *Scientific Reports*, 7(1):1–14, 2017.
- [35] Qiang Liu and Dilin Wang. Stein variational gradient descent: A general purpose Bayesian inference algorithm. In *Advances in Neural Information Processing Systems*, pages 2378–2386, 2016.
- [36] Christos Louizos and Max Welling. Structured and efficient variational deep learning with matrix gaussian posteriors. In *International Conference on Machine Learning*, pages 1708–1716, 2016.
- [37] David JC MacKay. A practical Bayesian framework for backpropagation networks. *Neural Computation*, 4(3):448–472, 1992.
- [38] David John Cameron Mackay. *Bayesian methods for adaptive models*. PhD thesis, California Institute of Technology, 1992.
- [39] Wesley J Maddox, Pavel Izmailov, Timur Garipov, Dmitry P Vetrov, and Andrew Gordon Wilson. A simple baseline for bayesian uncertainty in deep learning. In *Advances in Neural Information Processing Systems*, pages 13153–13164, 2019.
- [40] James Martens and Roger Grosse. Optimizing neural networks with kronecker-factored approximate curvature. In *International Conference on Machine Learning*, pages 2408–2417. PMLR, 2015.
- [41] Andres Masegosa. Learning under model misspecification: Applications to variational and ensemble methods. *Advances in Neural Information Processing Systems*, 33:5479–5491, 2020.
- [42] J Mercer. Functions of positive and negative type and their connection with the theory of integral equations. *Philosophical Transactions of the Royal Society*, pages 4–415, 1909.
- [43] Marina Munkhoeva, Yermek Kapushev, Evgeny Burnaev, and Ivan Oseledets. Quadrature-based features for kernel approximation. *Advances in Neural Information Processing Systems*, 31, 2018.
- [44] Radford M Neal. *Bayesian Learning for Neural Networks*. PhD thesis, University of Toronto, 1995.
- [45] Evert J Nyström. Über die praktische auflösung von integralgleichungen mit anwendungen auf randwertaufgaben. *Acta Mathematica*, 54:185–204, 1930.
- [46] Kazuki Osawa, Siddharth Swaroop, Anirudh Jain, Runa Eschenhagen, Richard E Turner, Rio Yokota, and Mohammad Emtiyaz Khan. Practical deep learning with Bayesian principles. *arXiv preprint arXiv:1906.02506*, 2019.
- [47] Adam Paszke, Sam Gross, Francisco Massa, Adam Lerer, James Bradbury, Gregory Chanan, Trevor Killeen, Zeming Lin, Natalia Gimelshein, Luca Antiga, et al. Pytorch: An imperative style, high-performance deep learning library. In *Advances in Neural Information Processing Systems*, pages 8026–8037, 2019.

- [48] Ali Rahimi and Benjamin Recht. Random features for large-scale kernel machines. *Advances in Neural Information Processing Systems*, 20, 2007.
- [49] Ali Rahimi and Benjamin Recht. Weighted sums of random kitchen sinks: Replacing minimization with randomization in learning. *Advances in Neural Information Processing Systems*, 21, 2008.
- [50] Hippolyt Ritter, Aleksandar Botev, and David Barber. A scalable laplace approximation for neural networks. In *6th International Conference on Learning Representations*, volume 6. International Conference on Representation Learning, 2018.
- [51] Matthias Seeger. Gaussian processes for machine learning. *International journal of neural systems*, 14(02):69–106, 2004.
- [52] Shengyang Sun, Changyou Chen, and Lawrence Carin. Learning structured weight uncertainty in Bayesian neural networks. In *International Conference on Artificial Intelligence and Statistics*, pages 1283–1292, 2017.
- [53] Michalis Titsias. Variational learning of inducing variables in sparse gaussian processes. In *International Conference on Artificial Intelligence and Statistics*, pages 567–574. PMLR, 2009.
- [54] Ashish Vaswani, Noam Shazeer, Niki Parmar, Jakob Uszkoreit, Llion Jones, Aidan N Gomez, Łukasz Kaiser, and Illia Polosukhin. Attention is all you need. In *Advances in Neural Information Processing Systems*, pages 5998–6008, 2017.
- [55] Max Welling and Yee W Teh. Bayesian learning via stochastic gradient langevin dynamics. In *International Conference on Machine Learning*, pages 681–688, 2011.
- [56] Yeming Wen, Paul Vicol, Jimmy Ba, Dustin Tran, and Roger Grosse. Flipout: Efficient pseudo-independent weight perturbations on mini-batches. *arXiv preprint arXiv:1803.04386*, 2018.
- [57] Veit Wild, Motonobu Kanagawa, and Dino Sejdinovic. Connections and equivalences between the nyström method and sparse variational gaussian processes. *arXiv preprint arXiv:2106.01121*, 2021.
- [58] Christopher Williams and Matthias Seeger. Using the nyström method to speed up kernel machines. *Advances in Neural Information Processing Systems*, 13, 2000.
- [59] Andrew Gordon Wilson and Pavel Izmailov. Bayesian deep learning and a probabilistic perspective of generalization. *arXiv preprint arXiv:2002.08791*, 2020.
- [60] Max A Woodbury. *Inverting modified matrices*. Statistical Research Group, 1950.
- [61] Felix Xinnan X Yu, Ananda Theertha Suresh, Krzysztof M Choromanski, Daniel N Holtmann-Rice, and Sanjiv Kumar. Orthogonal random features. *Advances in Neural Information Processing Systems*, 29, 2016.
- [62] Guodong Zhang, Shengyang Sun, David Duvenaud, and Roger Grosse. Noisy natural gradient as variational inference. In *International Conference on Machine Learning*, pages 5847–5856, 2018.
- [63] Ruqi Zhang, Chunyuan Li, Jianyi Zhang, Changyou Chen, and Andrew Gordon Wilson. Cyclical stochastic gradient mcmc for bayesian deep learning. *arXiv preprint arXiv:1902.03932*, 2019.

Checklist

1. For all authors...
 - (a) Do the main claims made in the abstract and introduction accurately reflect the paper’s contributions and scope? [\[Yes\]](#)
 - (b) Did you describe the limitations of your work? [\[Yes\]](#) See Section Related Work.
 - (c) Did you discuss any potential negative societal impacts of your work? [\[N/A\]](#)
 - (d) Have you read the ethics review guidelines and ensured that your paper conforms to them? [\[Yes\]](#)
2. If you are including theoretical results...
 - (a) Did you state the full set of assumptions of all theoretical results? [\[N/A\]](#)
 - (b) Did you include complete proofs of all theoretical results? [\[Yes\]](#) See Appendix.
3. If you ran experiments...
 - (a) Did you include the code, data, and instructions needed to reproduce the main experimental results (either in the supplemental material or as a URL)? [\[Yes\]](#) See supplemental material.
 - (b) Did you specify all the training details (e.g., data splits, hyperparameters, how they were chosen)? [\[Yes\]](#) See Section Experiments.

- (c) Did you report error bars (e.g., with respect to the random seed after running experiments multiple times)? [No]
 - (d) Did you include the total amount of compute and the type of resources used (e.g., type of GPUs, internal cluster, or cloud provider)? [No]
4. If you are using existing assets (e.g., code, data, models) or curating/releasing new assets...
- (a) If your work uses existing assets, did you cite the creators? [Yes]
 - (b) Did you mention the license of the assets? [N/A]
 - (c) Did you include any new assets either in the supplemental material or as a URL? [No]
 - (d) Did you discuss whether and how consent was obtained from people whose data you're using/curating? [N/A]
 - (e) Did you discuss whether the data you are using/curating contains personally identifiable information or offensive content? [N/A]
5. If you used crowdsourcing or conducted research with human subjects...
- (a) Did you include the full text of instructions given to participants and screenshots, if applicable? [N/A]
 - (b) Did you describe any potential participant risks, with links to Institutional Review Board (IRB) approvals, if applicable? [N/A]
 - (c) Did you include the estimated hourly wage paid to participants and the total amount spent on participant compensation? [N/A]

A Proof

A.1 Derivation of Equation (5)

Given

$$\Sigma = \sigma_0^2 \left(\mathbf{I}_P - \mathbf{J}_{\hat{\theta}, \mathbf{X}}^\top \left[\Lambda_{\mathbf{X}, \mathbf{Y}}^{-1} / \sigma_0^2 + \mathbf{J}_{\hat{\theta}, \mathbf{X}} \mathbf{J}_{\hat{\theta}, \mathbf{X}}^\top \right]^{-1} \mathbf{J}_{\hat{\theta}, \mathbf{X}} \right),$$

we have

$$\begin{aligned} \kappa_{\text{LLA}}(\mathbf{x}, \mathbf{x}') &= \mathbf{J}_{\hat{\theta}}(\mathbf{x}) \Sigma \mathbf{J}_{\hat{\theta}}(\mathbf{x}')^\top \\ &= \sigma_0^2 \mathbf{J}_{\hat{\theta}}(\mathbf{x}) \left(\mathbf{I}_P - \mathbf{J}_{\hat{\theta}, \mathbf{X}}^\top \left[\Lambda_{\mathbf{X}, \mathbf{Y}}^{-1} / \sigma_0^2 + \mathbf{J}_{\hat{\theta}, \mathbf{X}} \mathbf{J}_{\hat{\theta}, \mathbf{X}}^\top \right]^{-1} \mathbf{J}_{\hat{\theta}, \mathbf{X}} \right) \mathbf{J}_{\hat{\theta}}(\mathbf{x}')^\top \\ &= \sigma_0^2 \left(\mathbf{J}_{\hat{\theta}}(\mathbf{x}) \mathbf{J}_{\hat{\theta}}(\mathbf{x}')^\top - \mathbf{J}_{\hat{\theta}}(\mathbf{x}) \mathbf{J}_{\hat{\theta}, \mathbf{X}}^\top \left[\Lambda_{\mathbf{X}, \mathbf{Y}}^{-1} / \sigma_0^2 + \mathbf{J}_{\hat{\theta}, \mathbf{X}} \mathbf{J}_{\hat{\theta}, \mathbf{X}}^\top \right]^{-1} \mathbf{J}_{\hat{\theta}, \mathbf{X}} \mathbf{J}_{\hat{\theta}}(\mathbf{x}')^\top \right) \\ &= \sigma_0^2 \left(\kappa_{\text{NTK}}(\mathbf{x}, \mathbf{x}') - \kappa_{\text{NTK}}(\mathbf{x}, \mathbf{X}) \left[\Lambda_{\mathbf{X}, \mathbf{Y}}^{-1} / \sigma_0^2 + \kappa_{\text{NTK}}(\mathbf{X}, \mathbf{X}) \right]^{-1} \kappa_{\text{NTK}}(\mathbf{X}, \mathbf{x}') \right). \end{aligned}$$

A.2 Derivation of Equation (6)

$$\begin{aligned} \kappa_{\text{ELLA}}(\mathbf{x}, \mathbf{x}') &= \sigma_0^2 \left(\varphi(\mathbf{x}) \varphi(\mathbf{x}')^\top - \varphi(\mathbf{x}) \varphi_{\mathbf{X}}^\top \left[\Lambda_{\mathbf{X}, \mathbf{Y}}^{-1} / \sigma_0^2 + \varphi_{\mathbf{X}} \varphi_{\mathbf{X}}^\top \right]^{-1} \varphi_{\mathbf{X}} \varphi(\mathbf{x}')^\top \right) \\ &= \varphi(\mathbf{x}) \sigma_0^2 \left(\mathbf{I}_K - \varphi_{\mathbf{X}}^\top \left[\Lambda_{\mathbf{X}, \mathbf{Y}}^{-1} / \sigma_0^2 + \varphi_{\mathbf{X}} \varphi_{\mathbf{X}}^\top \right]^{-1} \varphi_{\mathbf{X}} \right) \varphi(\mathbf{x}')^\top \\ &= \varphi(\mathbf{x}) \left[\varphi_{\mathbf{X}}^\top \Lambda_{\mathbf{X}, \mathbf{Y}} \varphi_{\mathbf{X}} + \mathbf{I}_K / \sigma_0^2 \right]^{-1} \varphi(\mathbf{x}')^\top \quad (\text{Woodbury matrix identity}) \\ &= \varphi(\mathbf{x}) \left[\sum_i \varphi(\mathbf{x}_i)^\top \Lambda(\mathbf{x}_i, \mathbf{y}_i) \varphi(\mathbf{x}_i) + \mathbf{I}_K / \sigma_0^2 \right]^{-1} \varphi(\mathbf{x}')^\top. \end{aligned}$$

A.3 Derivation of Equation (18)

When $M = K$, the eigenvalues and eigenvectors of $\mathbf{K} = \mathbf{J}_{\hat{\theta}, \bar{\mathbf{X}}} \mathbf{J}_{\hat{\theta}, \bar{\mathbf{X}}}^\top$ can be organized as square matrices $\text{diag}(\boldsymbol{\lambda}) = \text{diag}(\lambda_1, \dots, \lambda_K)$ and $\mathbf{U} = [\mathbf{u}_1, \dots, \mathbf{u}_K]$ respectively. And $\varphi(\mathbf{x}) = [J_{\hat{\theta}}(\mathbf{x})v_1, \dots, J_{\hat{\theta}}(\mathbf{x})v_K] = J_{\hat{\theta}}(\mathbf{x}) \mathbf{J}_{\hat{\theta}, \bar{\mathbf{X}}}^\top \mathbf{U} \text{diag}(\boldsymbol{\lambda})^{-\frac{1}{2}}$. Of note that \mathbf{U} is a orthogonal matrix where $\mathbf{U}\mathbf{U}^\top = \mathbf{U}^\top \mathbf{U} = \mathbf{I}_K \Rightarrow \mathbf{U}^{-1} = \mathbf{U}^\top$, and by definition, $\mathbf{J}_{\hat{\theta}, \bar{\mathbf{X}}} \mathbf{J}_{\hat{\theta}, \bar{\mathbf{X}}}^\top = \mathbf{U} \text{diag}(\boldsymbol{\lambda}) \mathbf{U}^\top$. Then

$$\begin{aligned} \kappa_{\text{ELLA}}(\mathbf{x}, \mathbf{x}') &= \varphi(\mathbf{x}) \left[\sum_i \varphi(\mathbf{x}_i)^\top \Lambda(\mathbf{x}_i, \mathbf{y}_i) \varphi(\mathbf{x}_i) + \mathbf{I}_K / \sigma_0^2 \right]^{-1} \varphi(\mathbf{x}')^\top \\ &= \varphi(\mathbf{x}) \left[\varphi_{\mathbf{X}}^\top \Lambda_{\mathbf{X}, \mathbf{Y}} \varphi_{\mathbf{X}} + \mathbf{I}_K / \sigma_0^2 \right]^{-1} \varphi(\mathbf{x}')^\top \\ &= J_{\hat{\theta}}(\mathbf{x}) \mathbf{J}_{\hat{\theta}, \bar{\mathbf{X}}}^\top \mathbf{U} \text{diag}(\boldsymbol{\lambda})^{-\frac{1}{2}} \left[\text{diag}(\boldsymbol{\lambda})^{-\frac{1}{2}} \mathbf{U}^\top \mathbf{J}_{\hat{\theta}, \bar{\mathbf{X}}} \mathbf{J}_{\hat{\theta}, \mathbf{X}}^\top \Lambda_{\mathbf{X}, \mathbf{Y}} \mathbf{J}_{\hat{\theta}, \mathbf{X}} \mathbf{J}_{\hat{\theta}, \bar{\mathbf{X}}}^\top \mathbf{U} \text{diag}(\boldsymbol{\lambda})^{-\frac{1}{2}} \right. \\ &\quad \left. + \mathbf{I}_K / \sigma_0^2 \right]^{-1} \text{diag}(\boldsymbol{\lambda})^{-\frac{1}{2}} \mathbf{U}^\top \mathbf{J}_{\hat{\theta}, \bar{\mathbf{X}}} J_{\hat{\theta}}(\mathbf{x}')^\top \\ &= J_{\hat{\theta}}(\mathbf{x}) \mathbf{J}_{\hat{\theta}, \bar{\mathbf{X}}}^\top \mathbf{U} \left[\mathbf{U}^\top \mathbf{J}_{\hat{\theta}, \bar{\mathbf{X}}} \mathbf{J}_{\hat{\theta}, \mathbf{X}}^\top \Lambda_{\mathbf{X}, \mathbf{Y}} \mathbf{J}_{\hat{\theta}, \mathbf{X}} \mathbf{J}_{\hat{\theta}, \bar{\mathbf{X}}}^\top \mathbf{U} + \text{diag}(\boldsymbol{\lambda}) / \sigma_0^2 \right]^{-1} \mathbf{U}^\top \mathbf{J}_{\hat{\theta}, \bar{\mathbf{X}}} J_{\hat{\theta}}(\mathbf{x}')^\top \\ &= J_{\hat{\theta}}(\mathbf{x}) \mathbf{J}_{\hat{\theta}, \bar{\mathbf{X}}}^\top \left[\mathbf{U}\mathbf{U}^\top \mathbf{J}_{\hat{\theta}, \bar{\mathbf{X}}} \mathbf{J}_{\hat{\theta}, \mathbf{X}}^\top \Lambda_{\mathbf{X}, \mathbf{Y}} \mathbf{J}_{\hat{\theta}, \mathbf{X}} \mathbf{J}_{\hat{\theta}, \bar{\mathbf{X}}}^\top \mathbf{U}\mathbf{U}^\top + \mathbf{U} \text{diag}(\boldsymbol{\lambda}) \mathbf{U}^\top / \sigma_0^2 \right]^{-1} \mathbf{J}_{\hat{\theta}, \bar{\mathbf{X}}} J_{\hat{\theta}}(\mathbf{x}')^\top \\ &= J_{\hat{\theta}}(\mathbf{x}) \mathbf{J}_{\hat{\theta}, \bar{\mathbf{X}}}^\top \left[\mathbf{J}_{\hat{\theta}, \bar{\mathbf{X}}} \mathbf{J}_{\hat{\theta}, \mathbf{X}}^\top \Lambda_{\mathbf{X}, \mathbf{Y}} \mathbf{J}_{\hat{\theta}, \mathbf{X}} \mathbf{J}_{\hat{\theta}, \bar{\mathbf{X}}}^\top + \mathbf{J}_{\hat{\theta}, \bar{\mathbf{X}}} \mathbf{J}_{\hat{\theta}, \bar{\mathbf{X}}}^\top / \sigma_0^2 \right]^{-1} \mathbf{J}_{\hat{\theta}, \bar{\mathbf{X}}} J_{\hat{\theta}}(\mathbf{x}')^\top. \end{aligned}$$

A.4 Proof of Theorem 1

Theorem 1. Let c_Λ be a finite constant associated with Λ , and \mathcal{E}' the error of Nyström approximation $\|\mathbf{J}_{\hat{\theta}, \mathbf{X}} \mathbf{J}_{\hat{\theta}, \bar{\mathbf{X}}}^\top (\mathbf{J}_{\hat{\theta}, \bar{\mathbf{X}}} \mathbf{J}_{\hat{\theta}, \bar{\mathbf{X}}}^\top)^{-1} \mathbf{J}_{\hat{\theta}, \bar{\mathbf{X}}} \mathbf{J}_{\hat{\theta}, \mathbf{X}}^\top - \mathbf{J}_{\hat{\theta}, \mathbf{X}} \mathbf{J}_{\hat{\theta}, \mathbf{X}}^\top\|$. It holds that

$$\mathcal{E} \leq \sigma_0^4 c_\Lambda \mathcal{E}' + \sigma_0^2.$$

Proof. With $\mathbf{K} = \mathbf{J}_{\hat{\theta}, \bar{\mathbf{x}}} \mathbf{J}_{\hat{\theta}, \bar{\mathbf{x}}}^\top \succ 0$, let $\mathbf{P} = \mathbf{J}_{\hat{\theta}, \bar{\mathbf{x}}}^\top \mathbf{K}^{-1} \mathbf{J}_{\hat{\theta}, \bar{\mathbf{x}}}$. By Woodbury matrix identity,

$$\begin{aligned} \Sigma' &= \mathbf{J}_{\hat{\theta}, \bar{\mathbf{x}}}^\top \left[\mathbf{J}_{\hat{\theta}, \bar{\mathbf{x}}} \mathbf{J}_{\hat{\theta}, \mathbf{X}}^\top \Lambda_{\mathbf{X}, \mathbf{Y}} \mathbf{J}_{\hat{\theta}, \mathbf{X}} \mathbf{J}_{\hat{\theta}, \bar{\mathbf{x}}}^\top + \mathbf{J}_{\hat{\theta}, \bar{\mathbf{x}}} \mathbf{J}_{\hat{\theta}, \bar{\mathbf{x}}}^\top / \sigma_0^2 \right]^{-1} \mathbf{J}_{\hat{\theta}, \bar{\mathbf{x}}} \\ &= \mathbf{J}_{\hat{\theta}, \bar{\mathbf{x}}}^\top \left[\mathbf{J}_{\hat{\theta}, \bar{\mathbf{x}}} \mathbf{J}_{\hat{\theta}, \mathbf{X}}^\top \Lambda_{\mathbf{X}, \mathbf{Y}} \mathbf{J}_{\hat{\theta}, \mathbf{X}} \mathbf{J}_{\hat{\theta}, \bar{\mathbf{x}}}^\top + \mathbf{K} / \sigma_0^2 \right]^{-1} \mathbf{J}_{\hat{\theta}, \bar{\mathbf{x}}} \\ &= \sigma_0^2 \mathbf{J}_{\hat{\theta}, \bar{\mathbf{x}}}^\top \left[\mathbf{K}^{-1} - \mathbf{K}^{-1} \mathbf{J}_{\hat{\theta}, \bar{\mathbf{x}}} \mathbf{J}_{\hat{\theta}, \mathbf{X}}^\top (\Lambda_{\bar{\mathbf{X}}, \mathbf{Y}}^{-1} / \sigma_0^2 + \mathbf{J}_{\hat{\theta}, \mathbf{X}} \mathbf{J}_{\hat{\theta}, \bar{\mathbf{x}}}^\top \mathbf{K}^{-1} \mathbf{J}_{\hat{\theta}, \bar{\mathbf{x}}} \mathbf{J}_{\hat{\theta}, \mathbf{X}}^\top)^{-1} \mathbf{J}_{\hat{\theta}, \mathbf{X}} \mathbf{J}_{\hat{\theta}, \bar{\mathbf{x}}}^\top \mathbf{K}^{-1} \right] \mathbf{J}_{\hat{\theta}, \bar{\mathbf{x}}} \\ &= \sigma_0^2 \left[\mathbf{P} - \mathbf{P} \mathbf{J}_{\hat{\theta}, \mathbf{X}}^\top (\Lambda_{\bar{\mathbf{X}}, \mathbf{Y}}^{-1} / \sigma_0^2 + \mathbf{J}_{\hat{\theta}, \mathbf{X}} \mathbf{P} \mathbf{J}_{\hat{\theta}, \mathbf{X}}^\top)^{-1} \mathbf{J}_{\hat{\theta}, \mathbf{X}} \mathbf{P} \right]. \end{aligned}$$

It is interesting to see that \mathbf{P} is a projector: $\mathbf{P}^2 = \mathbf{P}$ and $\mathbf{P} \mathbf{J}_{\hat{\theta}, \bar{\mathbf{x}}}^\top = \mathbf{J}_{\hat{\theta}, \bar{\mathbf{x}}}^\top$. Then

$$\Sigma' = \sigma_0^2 \left[\mathbf{P} - \mathbf{P} \mathbf{J}_{\hat{\theta}, \mathbf{X}}^\top (\Lambda_{\bar{\mathbf{X}}, \mathbf{Y}}^{-1} / \sigma_0^2 + \mathbf{J}_{\hat{\theta}, \mathbf{X}} \mathbf{P} \mathbf{J}_{\hat{\theta}, \mathbf{X}}^\top)^{-1} \mathbf{J}_{\hat{\theta}, \mathbf{X}} \mathbf{P} \right].$$

By Woodbury matrix identity again,

$$\begin{aligned} \Sigma' &= \sigma_0^2 \left[\mathbf{P} - \sigma_0^2 \mathbf{P} \mathbf{J}_{\hat{\theta}, \mathbf{X}}^\top \left(\Lambda_{\mathbf{X}, \mathbf{Y}} - \Lambda_{\mathbf{X}, \mathbf{Y}} \mathbf{J}_{\hat{\theta}, \mathbf{X}} \mathbf{P} (\mathbf{I}_P / \sigma_0^2 \right. \right. \\ &\quad \left. \left. + \mathbf{P} \mathbf{J}_{\hat{\theta}, \mathbf{X}}^\top \Lambda_{\mathbf{X}, \mathbf{Y}} \mathbf{J}_{\hat{\theta}, \mathbf{X}} \mathbf{P})^{-1} \mathbf{P} \mathbf{J}_{\hat{\theta}, \mathbf{X}}^\top \Lambda_{\mathbf{X}, \mathbf{Y}} \right) \mathbf{J}_{\hat{\theta}, \mathbf{X}} \mathbf{P} \right] \\ &= \sigma_0^2 \left[\mathbf{P} - \sigma_0^2 \left(\mathbf{P} \mathbf{J}_{\hat{\theta}, \mathbf{X}}^\top \Lambda_{\mathbf{X}, \mathbf{Y}} \mathbf{J}_{\hat{\theta}, \mathbf{X}} \mathbf{P} - \mathbf{P} \mathbf{J}_{\hat{\theta}, \mathbf{X}}^\top \Lambda_{\mathbf{X}, \mathbf{Y}} \mathbf{J}_{\hat{\theta}, \mathbf{X}} \mathbf{P} (\mathbf{I}_P / \sigma_0^2 \right. \right. \\ &\quad \left. \left. + \mathbf{P} \mathbf{J}_{\hat{\theta}, \mathbf{X}}^\top \Lambda_{\mathbf{X}, \mathbf{Y}} \mathbf{J}_{\hat{\theta}, \mathbf{X}} \mathbf{P})^{-1} \mathbf{P} \mathbf{J}_{\hat{\theta}, \mathbf{X}}^\top \Lambda_{\mathbf{X}, \mathbf{Y}} \mathbf{J}_{\hat{\theta}, \mathbf{X}} \mathbf{P} \right) \right]. \end{aligned}$$

Let $\mathbf{T} = (\mathbf{P} \mathbf{J}_{\hat{\theta}, \mathbf{X}}^\top \Lambda_{\mathbf{X}, \mathbf{Y}} \mathbf{J}_{\hat{\theta}, \mathbf{X}} \mathbf{P} + \mathbf{I}_P / \sigma_0^2)^{-1}$, so $\mathbf{P} \mathbf{J}_{\hat{\theta}, \mathbf{X}}^\top \Lambda_{\mathbf{X}, \mathbf{Y}} \mathbf{J}_{\hat{\theta}, \mathbf{X}} \mathbf{P} = \mathbf{T}^{-1} - \mathbf{I}_P / \sigma_0^2$. It follows that

$$\Sigma' = \sigma_0^2 \left[\mathbf{P} - \sigma_0^2 \left(\mathbf{T}^{-1} - \mathbf{I}_P / \sigma_0^2 - (\mathbf{T}^{-1} - \mathbf{I}_P / \sigma_0^2) \mathbf{T} (\mathbf{T}^{-1} - \mathbf{I}_P / \sigma_0^2) \right) \right] = \mathbf{T} + \sigma_0^2 (\mathbf{P} - \mathbf{I}_P).$$

As a result,

$$\begin{aligned} \mathcal{E} &= \|\Sigma' - \Sigma\| \\ &= \|\mathbf{T} + \sigma_0^2 (\mathbf{P} - \mathbf{I}_P) - \Sigma\| \\ &\leq \|\mathbf{T} - \Sigma\| + \sigma_0^2 \|\mathbf{P} - \mathbf{I}_P\| \\ &= \|\mathbf{T} - \Sigma\| + \sigma_0^2, \end{aligned}$$

where we leverage the fact that the eigenvalue of the projector \mathbf{P} is either 1 or 0. And

$$\begin{aligned} \|\mathbf{T} - \Sigma\| &= \|\mathbf{T} - \mathbf{T} (\mathbf{T}^{-1} - \Sigma^{-1}) \Sigma\| \\ &= \|\mathbf{T} - \mathbf{T} (\mathbf{P} \mathbf{J}_{\hat{\theta}, \mathbf{X}}^\top \Lambda_{\mathbf{X}, \mathbf{Y}} \mathbf{J}_{\hat{\theta}, \mathbf{X}} \mathbf{P} - \mathbf{J}_{\hat{\theta}, \mathbf{X}}^\top \Lambda_{\mathbf{X}, \mathbf{Y}} \mathbf{J}_{\hat{\theta}, \mathbf{X}}) \Sigma\| \\ &\leq \|\mathbf{T}\| \|\Sigma\| \|\mathbf{P} \mathbf{J}_{\hat{\theta}, \mathbf{X}}^\top \Lambda_{\mathbf{X}, \mathbf{Y}} \mathbf{J}_{\hat{\theta}, \mathbf{X}} \mathbf{P} - \mathbf{J}_{\hat{\theta}, \mathbf{X}}^\top \Lambda_{\mathbf{X}, \mathbf{Y}} \mathbf{J}_{\hat{\theta}, \mathbf{X}}\| \\ &\leq \frac{\|\mathbf{P} \mathbf{J}_{\hat{\theta}, \mathbf{X}}^\top \Lambda_{\mathbf{X}, \mathbf{Y}} \mathbf{J}_{\hat{\theta}, \mathbf{X}} \mathbf{P} - \mathbf{J}_{\hat{\theta}, \mathbf{X}}^\top \Lambda_{\mathbf{X}, \mathbf{Y}} \mathbf{J}_{\hat{\theta}, \mathbf{X}}\|}{\lambda_{\min}(\mathbf{P} \mathbf{J}_{\hat{\theta}, \mathbf{X}}^\top \Lambda_{\mathbf{X}, \mathbf{Y}} \mathbf{J}_{\hat{\theta}, \mathbf{X}} \mathbf{P} + \mathbf{I}_P / \sigma_0^2) \lambda_{\min}(\mathbf{J}_{\hat{\theta}, \mathbf{X}}^\top \Lambda_{\mathbf{X}, \mathbf{Y}} \mathbf{J}_{\hat{\theta}, \mathbf{X}} + \mathbf{I}_P / \sigma_0^2)} \\ &\leq \sigma_0^4 \|\mathbf{P} \mathbf{J}_{\hat{\theta}, \mathbf{X}}^\top \Lambda_{\mathbf{X}, \mathbf{Y}} \mathbf{J}_{\hat{\theta}, \mathbf{X}} \mathbf{P} - \mathbf{J}_{\hat{\theta}, \mathbf{X}}^\top \Lambda_{\mathbf{X}, \mathbf{Y}} \mathbf{J}_{\hat{\theta}, \mathbf{X}}\|, \end{aligned}$$

where $\lambda_{\min}(\cdot)$ denotes the smallest eigenvalue of a matrix. The last inequality holds due to that the eigenvalues of $\mathbf{P} \mathbf{J}_{\hat{\theta}, \mathbf{X}}^\top \Lambda_{\mathbf{X}, \mathbf{Y}} \mathbf{J}_{\hat{\theta}, \mathbf{X}} \mathbf{P} + \mathbf{I}_P / \sigma_0^2$ and $\mathbf{J}_{\hat{\theta}, \mathbf{X}}^\top \Lambda_{\mathbf{X}, \mathbf{Y}} \mathbf{J}_{\hat{\theta}, \mathbf{X}} + \mathbf{I}_P / \sigma_0^2$ are larger than or equal to $1 / \sigma_0^2$ as $\mathbf{P} \mathbf{J}_{\hat{\theta}, \mathbf{X}}^\top \Lambda_{\mathbf{X}, \mathbf{Y}} \mathbf{J}_{\hat{\theta}, \mathbf{X}} \mathbf{P}$ and $\mathbf{J}_{\hat{\theta}, \mathbf{X}}^\top \Lambda_{\mathbf{X}, \mathbf{Y}} \mathbf{J}_{\hat{\theta}, \mathbf{X}}$ are SPSD.

To estimate the upper bound of $\|\mathbf{T} - \Sigma\|$, we lay out the following Lemma.

Lemma 1 (Proposition of Weinstein–Aronszajn identity). *If \mathbf{A} and \mathbf{B} are matrices of size $m \times n$ and $n \times m$ respectively, the non-zero eigenvalues of $\mathbf{A}\mathbf{B}$ and $\mathbf{B}\mathbf{A}$ are the same.*

It follows that

$$\begin{aligned}
\|\mathbf{T} - \Sigma\| &\leq \sigma_0^4 \|\mathbf{P}\mathbf{J}_{\hat{\theta}, \mathbf{X}}^\top \Lambda_{\mathbf{X}, \mathbf{Y}} \mathbf{J}_{\hat{\theta}, \mathbf{X}} \mathbf{P} - \mathbf{J}_{\hat{\theta}, \mathbf{X}}^\top \Lambda_{\mathbf{X}, \mathbf{Y}} \mathbf{J}_{\hat{\theta}, \mathbf{X}}\| \\
&= \frac{\sigma_0^4}{2} \left\| (\mathbf{P}\mathbf{J}_{\hat{\theta}, \mathbf{X}}^\top \Lambda_{\mathbf{X}, \mathbf{Y}}^{\frac{1}{2}} + \mathbf{J}_{\hat{\theta}, \mathbf{X}}^\top \Lambda_{\mathbf{X}, \mathbf{Y}}^{\frac{1}{2}}) (\Lambda_{\mathbf{X}, \mathbf{Y}}^{\frac{1}{2}} \mathbf{J}_{\hat{\theta}, \mathbf{X}} \mathbf{P} - \Lambda_{\mathbf{X}, \mathbf{Y}}^{\frac{1}{2}} \mathbf{J}_{\hat{\theta}, \mathbf{X}}) \right. \\
&\quad \left. + (\mathbf{P}\mathbf{J}_{\hat{\theta}, \mathbf{X}}^\top \Lambda_{\mathbf{X}, \mathbf{Y}}^{\frac{1}{2}} - \mathbf{J}_{\hat{\theta}, \mathbf{X}}^\top \Lambda_{\mathbf{X}, \mathbf{Y}}^{\frac{1}{2}}) (\Lambda_{\mathbf{X}, \mathbf{Y}}^{\frac{1}{2}} \mathbf{J}_{\hat{\theta}, \mathbf{X}} \mathbf{P} + \Lambda_{\mathbf{X}, \mathbf{Y}}^{\frac{1}{2}} \mathbf{J}_{\hat{\theta}, \mathbf{X}}) \right\| \\
&\leq \frac{\sigma_0^4}{2} \left\| (\mathbf{P}\mathbf{J}_{\hat{\theta}, \mathbf{X}}^\top \Lambda_{\mathbf{X}, \mathbf{Y}}^{\frac{1}{2}} + \mathbf{J}_{\hat{\theta}, \mathbf{X}}^\top \Lambda_{\mathbf{X}, \mathbf{Y}}^{\frac{1}{2}}) (\Lambda_{\mathbf{X}, \mathbf{Y}}^{\frac{1}{2}} \mathbf{J}_{\hat{\theta}, \mathbf{X}} \mathbf{P} - \Lambda_{\mathbf{X}, \mathbf{Y}}^{\frac{1}{2}} \mathbf{J}_{\hat{\theta}, \mathbf{X}}) \right\| \\
&\quad + \frac{\sigma_0^4}{2} \left\| ((\mathbf{P}\mathbf{J}_{\hat{\theta}, \mathbf{X}}^\top \Lambda_{\mathbf{X}, \mathbf{Y}}^{\frac{1}{2}} + \mathbf{J}_{\hat{\theta}, \mathbf{X}}^\top \Lambda_{\mathbf{X}, \mathbf{Y}}^{\frac{1}{2}}) (\Lambda_{\mathbf{X}, \mathbf{Y}}^{\frac{1}{2}} \mathbf{J}_{\hat{\theta}, \mathbf{X}} \mathbf{P} - \Lambda_{\mathbf{X}, \mathbf{Y}}^{\frac{1}{2}} \mathbf{J}_{\hat{\theta}, \mathbf{X}}))^\top \right\| \\
&= \sigma_0^4 \left\| (\mathbf{P}\mathbf{J}_{\hat{\theta}, \mathbf{X}}^\top \Lambda_{\mathbf{X}, \mathbf{Y}}^{\frac{1}{2}} + \mathbf{J}_{\hat{\theta}, \mathbf{X}}^\top \Lambda_{\mathbf{X}, \mathbf{Y}}^{\frac{1}{2}}) (\Lambda_{\mathbf{X}, \mathbf{Y}}^{\frac{1}{2}} \mathbf{J}_{\hat{\theta}, \mathbf{X}} \mathbf{P} - \Lambda_{\mathbf{X}, \mathbf{Y}}^{\frac{1}{2}} \mathbf{J}_{\hat{\theta}, \mathbf{X}}) \right\| \quad (\|\mathbf{A}^\top\| = \|\mathbf{A}\|) \\
&= \sigma_0^4 \left\| (\mathbf{P} + \mathbf{I}_P) \mathbf{J}_{\hat{\theta}, \mathbf{X}}^\top \Lambda_{\mathbf{X}, \mathbf{Y}} \mathbf{J}_{\hat{\theta}, \mathbf{X}} (\mathbf{P} - \mathbf{I}_P) \right\| \\
&= \sigma_0^4 \left\| \Lambda_{\mathbf{X}, \mathbf{Y}} \mathbf{J}_{\hat{\theta}, \mathbf{X}} (\mathbf{P} - \mathbf{I}_P) (\mathbf{P} + \mathbf{I}_P) \mathbf{J}_{\hat{\theta}, \mathbf{X}}^\top \right\| \quad (\text{Lemma 1}) \\
&= \sigma_0^4 \left\| \Lambda_{\mathbf{X}, \mathbf{Y}} \mathbf{J}_{\hat{\theta}, \mathbf{X}} (\mathbf{P} - \mathbf{I}_P) \mathbf{J}_{\hat{\theta}, \mathbf{X}}^\top \right\| \quad (\mathbf{P}^2 = \mathbf{P}) \\
&= \sigma_0^4 \left\| \Lambda_{\mathbf{X}, \mathbf{Y}} (\mathbf{J}_{\hat{\theta}, \mathbf{X}} \mathbf{J}_{\hat{\theta}, \tilde{\mathbf{X}}}^\top (\mathbf{J}_{\hat{\theta}, \tilde{\mathbf{X}}} \mathbf{J}_{\hat{\theta}, \tilde{\mathbf{X}}}^\top)^{-1} \mathbf{J}_{\hat{\theta}, \tilde{\mathbf{X}}} \mathbf{J}_{\hat{\theta}, \mathbf{X}}^\top - \mathbf{J}_{\hat{\theta}, \mathbf{X}} \mathbf{J}_{\hat{\theta}, \mathbf{X}}^\top) \right\| \\
&\leq \sigma_0^4 \left\| \Lambda_{\mathbf{X}, \mathbf{Y}} \right\| \left\| \mathbf{J}_{\hat{\theta}, \mathbf{X}} \mathbf{J}_{\hat{\theta}, \tilde{\mathbf{X}}}^\top (\mathbf{J}_{\hat{\theta}, \tilde{\mathbf{X}}} \mathbf{J}_{\hat{\theta}, \tilde{\mathbf{X}}}^\top)^{-1} \mathbf{J}_{\hat{\theta}, \tilde{\mathbf{X}}} \mathbf{J}_{\hat{\theta}, \mathbf{X}}^\top - \mathbf{J}_{\hat{\theta}, \mathbf{X}} \mathbf{J}_{\hat{\theta}, \mathbf{X}}^\top \right\|.
\end{aligned}$$

It is easy to show that $\|\Lambda_{\mathbf{X}, \mathbf{Y}}\| \leq c_\Lambda$ with c_Λ as a finite constant. For example, when handling regression tasks, $-\log p(\mathbf{y}|\mathbf{g})$ typically boils down to $\frac{1}{2\sigma_{\text{noise}}^2}(\mathbf{g} - \mathbf{y})^\top(\mathbf{g} - \mathbf{y})$ where σ_{noise}^2 refers to the variance of data noise, so $-\nabla_{\mathbf{g}\mathbf{g}}^2 \log p(\mathbf{y}|\mathbf{g}) = \frac{1}{\sigma_{\text{noise}}^2} \mathbf{I}_C$ and $c_\Lambda = \frac{1}{\sigma_{\text{noise}}^2}$.

When facing classification cases, $-\log p(\mathbf{y}|\mathbf{g})$ becomes the softmax cross-entropy loss. It is guaranteed that $c_\Lambda \leq 2$ because

$$\begin{aligned}
\|-\nabla_{\mathbf{g}\mathbf{g}}^2 \log p(\mathbf{y}|\mathbf{g})\| &= \|\text{diag}(\text{softmax}(\mathbf{g})) - \text{softmax}(\mathbf{g})\text{softmax}(\mathbf{g})^\top\| \\
&\leq \|\text{diag}(\text{softmax}(\mathbf{g}))\| + \|\text{softmax}(\mathbf{g})\text{softmax}(\mathbf{g})^\top\| \\
&\leq 1 + \|\text{softmax}(\mathbf{g})^\top \text{softmax}(\mathbf{g})\| \leq 1 + 1 = 2.
\end{aligned}$$

To summarize, we have the following bound for the approximation error \mathcal{E} :

$$\mathcal{E} \leq \|\mathbf{T} - \Sigma\| + \sigma_0^2 = \sigma_0^4 c_\Lambda \left\| \mathbf{J}_{\hat{\theta}, \mathbf{X}} \mathbf{J}_{\hat{\theta}, \tilde{\mathbf{X}}}^\top (\mathbf{J}_{\hat{\theta}, \tilde{\mathbf{X}}} \mathbf{J}_{\hat{\theta}, \tilde{\mathbf{X}}}^\top)^{-1} \mathbf{J}_{\hat{\theta}, \tilde{\mathbf{X}}} \mathbf{J}_{\hat{\theta}, \mathbf{X}}^\top - \mathbf{J}_{\hat{\theta}, \mathbf{X}} \mathbf{J}_{\hat{\theta}, \mathbf{X}}^\top \right\| + \sigma_0^2.$$

□

B How Does ELLA Address the Scalability Issues of Nyström Approximation

Existing works like NeuralEF [9] highlight the scalability issues of the Nyström approximation when applied to NTKs, but they have been successfully addressed by ELLA, which reflects our technical novelty. On the one hand, the cost of eigendecomposing the $M \times M$ matrix in our case is low considering that we set $M < 10^4$. As shown in Figure 2(a)(b), $M = 2000$ can lead to reasonably small approximation errors for both the Nyström approximation and the resulting ELLA covariance. On the other hand, the prediction cost at test time is reduced by two innovations in this work. Firstly, looking at Equation (14), typical Nyström method first computes $J_{\hat{\theta}}(\mathbf{x}, i) \mathbf{J}_{\hat{\theta}, \tilde{\mathbf{X}}}^\top$ (i.e., evaluate the NTK similarities between (\mathbf{x}, i) and all training data $\tilde{\mathbf{X}}$) and then multiplies the result with $\mathbf{u}_k \in \mathbb{R}^M$ to get the evaluation of k -th eigenfunction. So it needs to store $\mathbf{J}_{\hat{\theta}, \tilde{\mathbf{X}}} \in \mathbb{R}^{M \times P}$ and compute M Jacobian-vector products (JVPs). But this work proposes to first compute $\mathbf{v}_k = \mathbf{J}_{\hat{\theta}, \tilde{\mathbf{X}}}^\top \mathbf{u}_k$, $k = 1, \dots, K$ (we omit the scalar multiplier) and then obtain the evaluation of k -th eigenfunction by $J_{\hat{\theta}}(\mathbf{x}, i) \mathbf{v}_k$. Namely, we only need to store K vectors of size P and compute K JVPs. In most cases, $M = 2000$ and $K = 20$, so the benefits of our technique are obvious. Secondly, we leverage forward-mode

Table 4: Test NLL of ELLA varies w.r.t. M and K ($M \geq K$) on CIFAR-10 with ResNet-20 architecture. The experiments for $K \geq 256$ are time-consuming so we have not included the corresponding results here.

$M \setminus K$	4	8	16	32	64	128
4	0.2689					
8	0.2690	0.2561				
16	0.2660	0.2548	0.2392			
32	0.2655	0.2541	0.2395	0.2318		
64	0.2672	0.2527	0.2398	0.2312	0.2299	
128	0.2674	0.2540	0.2383	0.2310	0.2298	0.2294
256	0.2679	0.2545	0.2382	0.2310	0.2300	0.2294
512	0.2678	0.2542	0.2376	0.2315	0.2292	0.2288
1024	0.2674	0.2545	0.2385	0.2314	0.2295	0.2292
2000	0.2673	0.2551	0.2380	0.2308	0.2301	0.2295

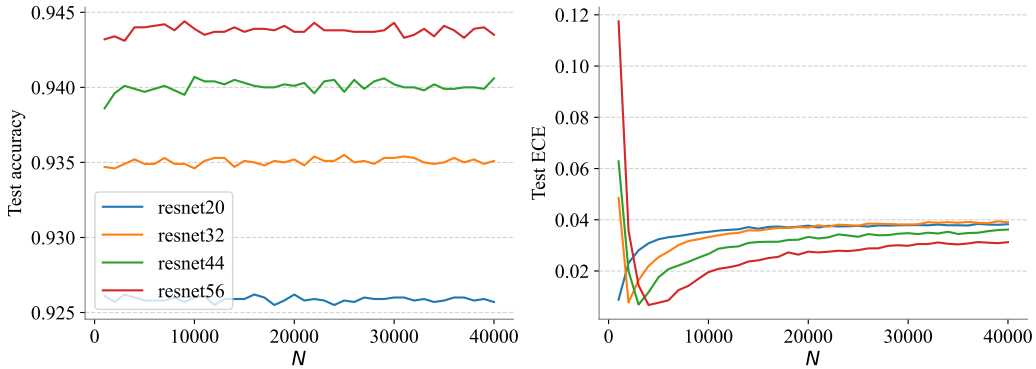


Figure 6: The test accuracy and ECE of ELLA vary w.r.t. the number of training data N on CIFAR-10.

autodiff (fwAD) to efficiently compute the JVPs where we do not need to explicitly compute and store the Jacobian $J_{\hat{\theta}}(\mathbf{x}, i)$ but to invoke once fwAD. Further, fwAD enables the parallel evaluation of JVPs over all output dimensions, i.e., we can concurrently compute $J_{\hat{\theta}}(\mathbf{x}, i)\mathbf{v}_k, i = 1, \dots, C$ in one forward pass. These techniques make the evaluation of ELLA equal to performing K forward passes under the scope of fwAD. This is similar to other BNNs that perform S forward passes with different MC parameter samples to estimate the posterior predictive.

C More Experimental Results

C.1 Test NLL of ELLA Varies w.r.t. K and M

Table 4 presents how the test NLL of ELLA varies w.r.t. M and K on CIFAR-10 with ResNet-20 architecture. Considering the results in Figure 2, we conclude that under the same K , a larger M can bring closer approximation but it does not necessarily lead to a better test NLL.

C.2 Test Accuracy and ECE of ELLA Vary w.r.t. N

Figure 6 presents how the test accuracy and ECE of ELLA vary w.r.t. the number of training data N on CIFAR-10.

C.3 Test NLL of LLA* Varies w.r.t. N

Figure 7 shows how the test NLL of LLA* varies w.r.t. the number of training data N on CIFAR-10. These results, as well as those in Section 5.2, reflect that the overfitting issue of LLA generally exists. We can also see that properly tuning the prior precision can alleviate the overfitting of LLA* to some extent but cannot fully resolve it.

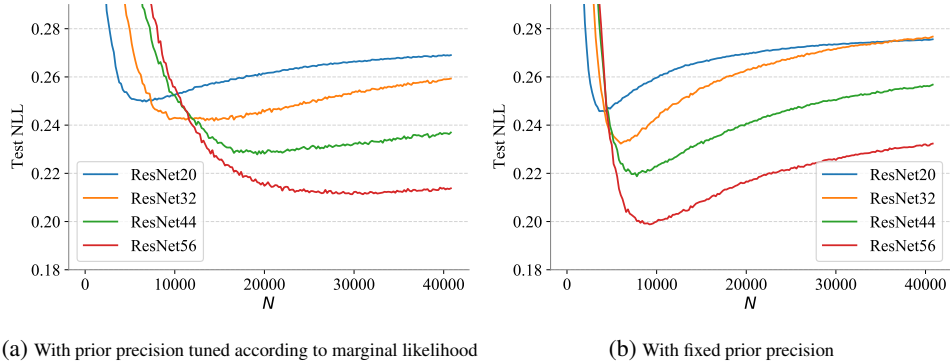


Figure 7: The test NLL of LLA* varies w.r.t. the number of training data N on CIFAR-10. The y axis is aligned with that of Figure 2(c).

Table 5: Comparison on the approximation error to vanilla LLA in the illustrative regression case, measured by the KL divergence between the predictive distributions.

	ELLA	LLA-KFAC	LLA-Diag	LLA*
KL div.	0.83	0.35	1.71	2.44

C.4 Comparison on the Approximation Error to Vanilla LLA

Table 5 lists the discrepancies between the predictive distributions of the approximate LLA method and vanilla LLA in the illustrative regression case detailed in Section 5.3. Here, considering the predictive distribution for one test datum is a Gaussian distribution, we use the KL divergence between the Gaussians yielded by the method of concern and LLA as a proxy of the approximation error (averaged over a set of test points).

C.5 More Results on CIFAR-10 Corruptions

Figure 8, Figure 9, and Figure 10 show the results of the considered methods on CIFAR-10 corruptions using ResNet-20, ResNet-32, and ResNet-44 architectures respectively. We can see that ELLA surpasses the baselines in aspects of NLL and ECE at various levels of skew. These results signify ELLA’s ability to make conservative predictions for OOD inputs.

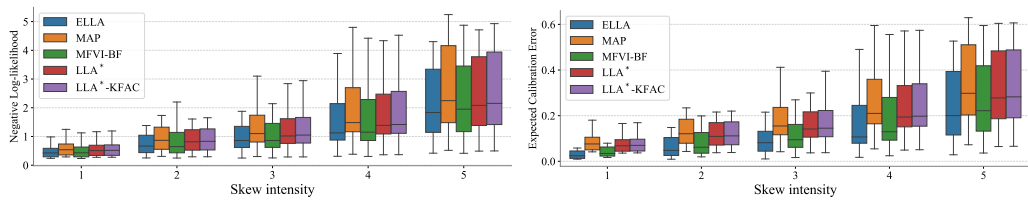


Figure 8: NLL (Left) and ECE (Right) on CIFAR-10 corruptions for models trained with ResNet-20 architecture. Each box corresponds to a summary of the results across 19 types of skew.

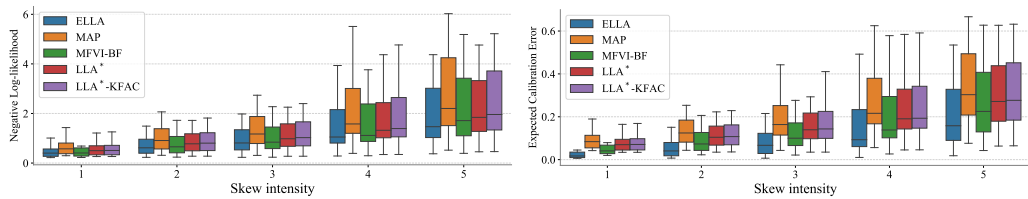


Figure 9: NLL (Left) and ECE (Right) on CIFAR-10 corruptions for models trained with ResNet-32 architecture. Each box corresponds to a summary of the results across 19 types of skew.

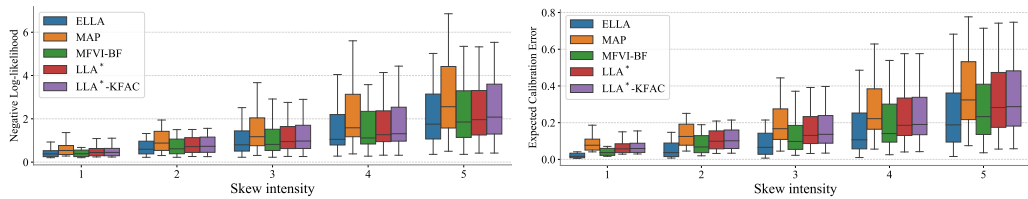


Figure 10: NLL (Left) and ECE (Right) on CIFAR-10 corruptions for models trained with ResNet-44 architecture. Each box corresponds to a summary of the results across 19 types of skew.